Structural basis to design multi-epitope vaccines against Novel Coronavirus 19 (COVID19) infection, the ongoing pandemic emergency: an in silico approach

Sukrit Srivastava*[a,b], Sonia Verma[c], Mohit Kamthania[d], Rupinder Kaur[e], Ruchi Kiran Badyal[f], Ajay Kumar Saxena[b], Ho-Joon Shin[g], Michael Kolbe[h,I], Kailash C Pandey[c]

a Department of Biotechnology, Institute of Bio-Medical Education and Research, Mangalayatan University, 202146 Aligarh, India.
b Molecular Medicine Lab., School of Life Science, Jawaharlal Nehru University, 110067 New Delhi, India.
c Parasite-Host Biology Group, Protein Biochemistry & Engineering Lab, ICMR-National Institute of Malaria Research, New Delhi, India
d Department of Biotechnology, Institute of Applied Medicines and Research, 201206 Ghaziabad, India.
e Department of Chemistry, Guru Nanak Dev University, Amritsar, India
f Department of economics, Mangalayata University, India
g Department of Microbiology,School of Medicine, Ajou University, South Korea
h Department for Structural Infection Biology, Centre for Structural Systems Biology (CSSB) & Helmholtz-Centre for Infection Research, Notkestraße 85, 22607 Hamburg, Germany.
i Faculty of Mathematics, Informatics and Natural Sciences, University of Hamburg, Rothenbaumchaussee 19, 20148 Hamburg, Germany.

*Correspondence should be addressed to S.S. (sukrit.srivastav@mangalayatan.edu.in; srivastav.sukrit@gmail.com)

Abstract

The 2019 novel coronavirus (COVID19 / Wuhan coronavirus), officially named as Severe Acute Respiratory Syndrome Coronavirus 2 (SARS-CoV-2), is a positive-sense single-stranded RNA coronavirus. SARS-CoV-2 causes the contagious

COVID19 disease also known as 2019-nCoV acute respiratory disease and has led to the ongoing 2019–20 pandemic COVID19 outbreak. The effective counter measures against SARS-CoV-2 infection require the design and development of specific and effective vaccine candidate. In the present study, we have screened and shortlisted 38 CTL, 33 HTL and 12 B cell epitopes from the eleven Protein sequences of SARS-CoV-2 by utilizing different in silico tools. The screened epitopes were further validated for their binding with their respective HLA allele binders and TAP (Transporter associated with antigen processing) molecule by molecular docking. The shortlisted screened epitopes were further utilized to design novel two multi-epitope vaccines (MEVs) composed of CTL, HTL and B cell epitopes overlaps with potential to elicit humoral as well as cellular immune response against SARS-CoV-2. To enhance the immune response for our vaccine design, truncated (residues 10-153) Onchocerca volvulus activation-associated secreted protein-1 (Ov-ASP-1) has been utilized as an adjuvant at N terminal of both the MEVs. Further molecular models for both the MEVs were prepared and validated for their stable molecular interactions with Toll-Like Receptor 3 (TLR 3). The codon-optimized cDNA of both the MEVs were further analyzed for their potential of high level of expression in a human cell line. The present study is very significant in terms of molecular designing of prospective CTL and HTL vaccine against SARS-CoV-2 infection with the potential to elicit cellular as well as humoral immune response.

Key words: COVID19, Severe Acute Respiratory Syndrome Coronavirus 2

(SARS-CoV-2), Coronavirus, Human Transporter associated with antigen processing (TAP), Toll-Like Receptor (TLR), Epitope, Immunoinformatics, Molecular Docking, Molecular dynamics simulation, Multi-epitope Vaccine

81
82
83
84
85
86
87
88
89
90
91
92
93
94
95
96
97
98
99
100
101
102
103

CTL Multi-epitope COVID19 vaccine - Toll Like Receptor 3 complex

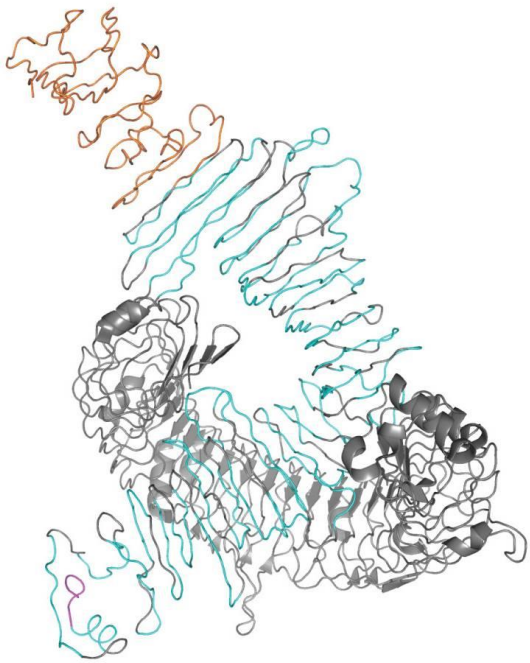

HTL Multi-epitope COVID19 vaccine - Toll Like Receptor 3 complex

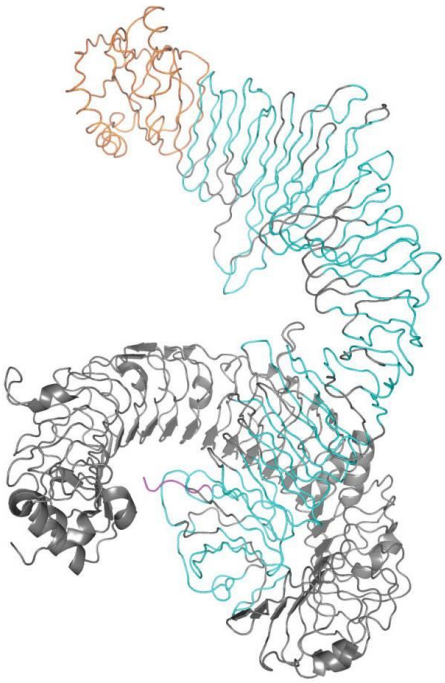

Graphical abstract: The designed CTL (Cytotoxic T lymphocyte) and HTL (Helper T lymphocyte) multi-epitope vaccines (MEV) against COVID19 infection. Both the CTL and HTL MEV models show a very stable and well fit conformational complex formation tendency with the Toll like receptor 3. CTL and HTL MEVs: *ribbon*; Toll like receptor 3: *gray cartoon*; Adjuvant [truncated (residues 10-153) Onchocerca volvulus activation-associated secreted protein-1]: *orange ribbon regions*; Epitopes: *cyan ribbons regions*; 6xHis Tag: *magenta ribbon regions.*

Abbreviations: Antigen-presenting cell (APCs), Codon Adaptation Index (CAI), Coronavirus ID 19 (COVID19), Coronavirus (CoV), Coverage (Cov), Cryo-Electron Microscopy (Cryo-EM), Cytotoxic T lymphocyte (CTL), ectodomain (ECD), Envelope Protein (E Protein), endoplasmic reticulum (ER), European Bioinformatics Institute (EBI), Nucleocapsid Protein (N Protein), Ope reading Frame (ORF), global distance test (GDT), Grand average of hydropathicity (GRAVY), root mean square deviation (RMSD), root mean square fluctuation (RMSF), Surface protein (S Protein), half maximal inhibitory concentration (IC50), Helper T lymphocyte (HTL), Human Leukocyte Antigen (HLA), Immune Epitope Database (IEDB), Immuno Polymorphism Database (IPD), Interferon Gama (IFN-γ), International ImMunoGeneTics project (IMGT), major histocompatibility complex (MHC), Membrane Protein (M Protein), Motif-EmeRging with ClassesIdentification (MERCI), Molecular dynamics simulation (MD simulation) Multi-epitope Vaccine (MEV), Multiple Sequence Alignment (MSA), non-structural

protein (nsp), National Center for Biotechnology Information (NCBI), peptide-MHC (pMHC), Severe Acute Respiratory Syndrome Coronavirus 2 (SARS-CoV-2), Stabilization Matrix alignment method (SMM), Transmembrane (TM), Protein Data Bank (PDB), Qualitative Model Energy ANalysis (QMEAN), root mean square deviation (RMSD), Support Vector Machine (SVM), Toll-Like Receptor 3 (TLR3), Transporter associated with antigen processing (TAP), un-normalized global distance test (uGDT), Yet Another Scientifc Artifcial Reality Application (YASARA)

Introduction

The novel coronavirus (COVID19), officially named as Severe Acute Respiratory Syndrome Coronavirus 2 (SARS-CoV-2) has caused the ongoing outbreak of a severe form of flu leading to death with a mortality rate of 3.4 %. The SARS-CoV-2 is a novel coronavirus associated with a respiratory disease initiated from the Wuhan of Hubei province, China. The disease is highly contagious and has spread to 182 countries/ Territories since its outbreak in China in December 2019 till 21st of March 2020. Worldwide, as of 21st March 2020, the total confirmed cases have been reported to be 2,66,073 and total death count reported is 11,184 (WHO Situation report 21st March 2020). Overall the SARS-CoV-2 infection has put a global emergency condition. The economic impact of COVID-19 is even harsher and has put the world on economic risk. As of 9th March, the downside scenario sees a $2 trillion shortfall in global income with a $220 billion hit to developing countries. The COVID-19 shock will cause a recession in

several countries and depress global annual growth this year to 2.5 percent lower, the recessionary threshold for the world economy (UNCTAD report 9th March 2020).

The infection mechanism and pathogenesis of SARS-CoV-2 is largely unknown yet. The proteome of SARS-CoV-2 is composed of 11 structural and non-structural proteins. These include polyprotein (ORF1ab), Surface protein (S Protein), ORF3, Envelope Protein (E Protein), Membrane Protein (M Protein), ORF6, ORF7a, ORF7b, ORF8, Nucleocapsid Protein (N Protein), and ORF10 (NCBI protein sequence database). The actual function and pathogenic or proliferative role of these SARS-CoV-2 coronavirus proteins are largely not known yet.

The SARS-CoV-2 coronavirus polyprotein (ORF1ab) with length of 7,096 amino acid (aa) is composed of 16 different expressed protein viz. leader protein (nsp1, location: 1-180 aa); nsp2 (location: 181-818); nsp3 (former nsp1, carry conserved domains - N-terminal acidic, predicted phosphoesterase, papain-like proteinase, Y-domain, transmembrane domain 1 (TM1) and adenosine diphosphate-ribose 1''-phosphatase, location: 819-2,763); nsp4 (contains transmembrane domain 2 (TM2), location: 2,764-3,263); 3C-like proteinase (nsp5, main proteinase, mediates cleavages downstream of nsp4, location: 3,264-3,569); nsp6 (putative transmembrane domain, location: 3,570-3,859); nsp7 (location: 3,860-3,942); nsp8 (location: 3,943-4,140); nsp9 (ssRNA-binding protein, location: 4,141-4,253); nsp10 (formerly known as growth-factor-like protein, location: 4,254-4,392); nsp11 (location: 4,393-4,405); RNA-dependent

RNA polymerase (nsp12, location: 4,393-5,324); Helicase (nsp13; zinc-binding domain, NTPase/helicase domain, RNA 5'-triphosphatase, location: 5,325-5,925); 3'-to-5' exonuclease (nsp14, location: 5,926-6,452); endo RNAse (nsp15, location: 6,453-6,798); and 2'-O-ribose methyltransferase (nsp16; location: 6,799-7,096).

The SARS-CoV-2 coronavirus surface glycoprotein (S Protein) is a structural protein and acts as spike protein, its location is 21,563-25,384 aa, and length is 1273 aa); The SARS-CoV-2 coronavirus ORF3a protein has location 25,393-26,220 aa and length 275 aa. The SARS-CoV-2 coronavirus envelope protein (E Protein) (ORF4) is a structural protein and has location 26,245-26,472 aa and length 75 aa. The SARS-CoV-2 coronavirus membrane glycoprotein (M Protein) (ORF5) is a structural protein and has location 26,523-27,191aa and length 222 aa. The SARS-CoV-2 coronavirus ORF6 protein has location 27,202-27,387 aa and length 61 aa. The SARS-CoV-2 coronavirus ORF7a protein has location 27,394-27,759 aa and length 121 aa. The SARS-CoV-2 coronavirus ORF7b protein has location 27,756-27,887 aa and length 43 aa. The SARS-CoV-2 coronavirus ORF8 protein has location 27,894-28,259 aa and length 121 aa. The SARS-CoV-2 coronavirus nucleocapsid phosphoprotein (N Protein) (ORF9) is a structural protein with location 28,274-29,533 aa and has a length of 419 aa. The SARS-CoV-2 coronavirus ORF10 protein has location 29,558-29,674 aa and length 38 aa (NCBI protein sequence database).

Although the exact mechanism and roles of all the above-mentioned proteins of SARS-CoV-2 coronavirus proteome are not well known yet, but these

proteins could act as potential vaccine candidates against the SARS-CoV-2 coronavirus infection. In the present study, we have screened highly potential epitopes from all the above-mentioned protein and further, we have also designed and proposed CTL (Cytotoxic T lymphocyte) and HTL (Helper T lymphocyte) multi-epitope based vaccine candidates against the SARS-CoV-2 coronavirus infection.

Methodology

In the present study on SARS-CoV-2 coronavirus, we have screened potential epitopes and have designed and proposed two multi-epitope vaccines (MEVs) composed of screened CTL (Cytotoxic T lymphocyte) and HTL (Helper T lymphocyte) epitopes with overlapping regions of B cell epitopes. Hence the proposed MEVs are supposed to have the potential to elicit both the humoral as well as cellular immune response. To enhance immune response, truncated (residues 10-153) Onchocerca volvulus activation-associated secreted protein-1 (Ov-ASP-1) has been utilized as an adjuvant at N-terminal of both the MEVs. The truncated Ov-ASP-1 was chosen due to its potential to activate antigen-processing cells (APCs) (MacDonald et al., 2005; Guo et al., 2015; He et al., 2009). All SARS-CoV-2 coronavirus proteins mentioned in the introduction were utilized to screen the potential CTL, HTL and B cell epitopes. The screened epitopes were further studied for overlapping consensus regions amongst them. The epitopes showing overlapping regions in partial or complete were chosen for detailed further studies.

The chosen CTL and HTL epitopes were analyzed for their molecular interaction with their respective HLA allele binders. Moreover, the chosen CTL epitopes were also analyzed for their molecular interaction with TAP (Transporter associated with antigen processing) transporter cavity to observe their smooth passage from cytoplasm to endoplasmic reticulum lumen (Oldham et al., 2016; Abele et al., 2004). The tertiary model for both MEVs were generated and refined. Both the MEVs models were further utilized to screened B Cell linear and discontinuous epitopes as well as IFN-γ inducing epitopes.

The molecular signaling by multiple TLRs, is an essential component of the innate immune response against SARS-CoV-2 coronavirus. Since the rOv-ASP-1 primarily binds APCs among human PBMCs and trigger pro-inflammatory cytokine production via Toll-like receptor 3 (TLR3), hence both the CTL and HTL MEV models were further analyzed for their molecular interaction with the TLR-3 by molecular docking studies (Antoniou et al., 2003; Delneste et al., 2007; Totura et al., 2015; Farina et al., 2005). Further, the codon- optimized cDNA of both the MEVs were analyzed to have a high level of expression in mammalian cell line (human), which would facilitate *in-vivo* expression, experimentation and trials (Fig.1).

Figure 1. Workflow chart.

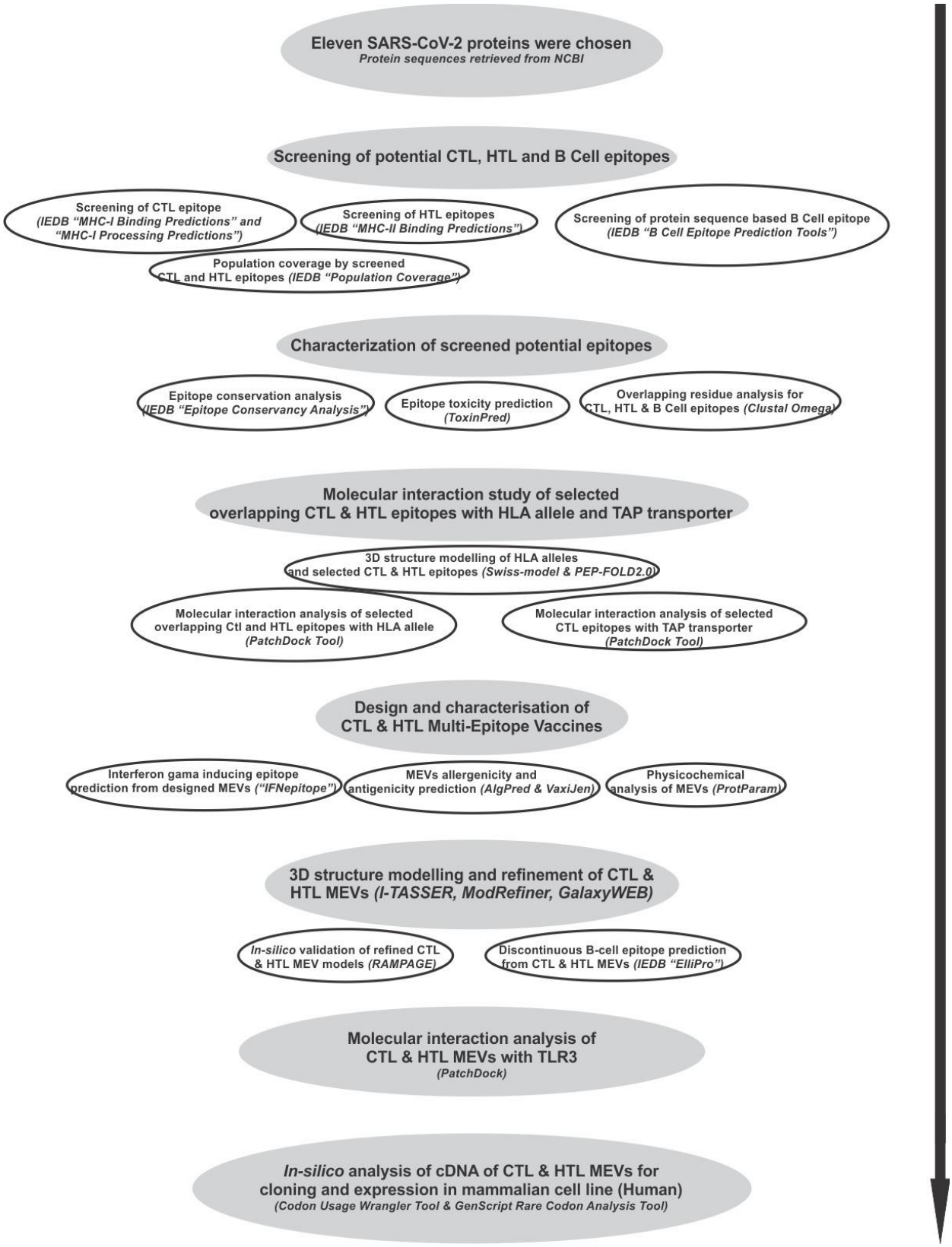

Screening of Potential Epitopes

T cell Epitope Prediction

Screening of Cytotoxic T lymphocyte (CTL) Epitope. The screening of Cytotoxic T lymphocyte epitopes was performed by the IEDB (Immune Epitope Database) tools "MHC-I Binding Predictions" (http://tools.iedb.org/mhci/) and "MHC-I Processing Predictions" (http://tools.iedb.org/processing/) (Tenzer et al., 2005; Peters et al., 2003; Hoof et al., 2009). Both the tools use six different methods (viz. Consensus, NN-align, SMM-align, Combinatorial library, Sturniolo and NetMHCIIpan) and generate "Percentile rank" and a "total score" respectively.

The screening is based on the total amount of cleavage sites in the protein. TAP score estimates an effective log -(IC50) values (half maximal inhibitory concentration (IC50) for binding to TAP of a peptide or its N-terminal prolonged precursors. The MHC binding prediction score is -log(IC50) values for binding to MHC of a peptide (Calis et al., 2013). The IC(50) (nM) value for each epitope and MHC allele binding pairs were also obtained by this IEDB tool. Epitopes having high, intermediate, and least affinity of binding to their HLA allele binders have IC50 values < 50 nM, < 500 nM and < 5000 nM, respectively.

Immunogenicity of all the screened CTL epitopes was also obtained by using "MHC I Immunogenicity" tool of IEDB (http://tools.iedb.org/immunogenicity/) with all the parameters set to default analyzing 1st, 2nd, and C-terminus amino acids of the given screened epitope (Calis et al., 2013). The tool predicts the immunogenicity of a given peptide-MHC (pMHC) complex based on the physiochemical properties of constituting amino

acid and their position within the peptide sequence.

Screening of Helper T lymphocyte (HTL) Epitopes. To screen out the Helper T lymphocyte epitopes from SARS-CoV-2 proteins, the IEDB tool "MHC-II Binding Predictions" (http://tools.iedb.org/mhcii/) was used. The tool generates "Percentile rank" for each potential peptide. The lower the value of percentile, higher would be the affinity. This percentile rank is generated by the combination of three different methods viz. combinatorial library, SMM_align & Sturniolo; and by comparing the score of the peptide against the scores of other random five million 15-mer peptides of SWISSPROT database (Wang et al., 2010; Sidney et al., 2008; Nielsen et al., 2007; Sturniolo et al., 1999). The rank from the consensus of all three methods was generated by the median percentile rank of the three methods.

Population Coverage by CTL and HTL epitopes. The "Population Coverage" tool of IEDB (http://tools.iedb.org/population/) was used to elucidate the world human population coverage by the shortlisted 38 CTL and 33 HTL epitopes derived from nine SARS-CoV-2 proteins (Bui et al., 2006). T cells recognize the complex between a specific major MHC molecule and a particular pathogen-derived epitope. The given epitope will elicit a response only in an individual that express an MHC molecule, which is capable of binding that particular epitope. This denominated MHC restriction of T cell responses and the MHC polymorphism provides the basis for population coverage study. The MHC types are expressed

311 at dramatically different frequencies in different ethnicities. Hence a vaccine with
312 larger population coverage could be of greater importance (Sturniolo et al.,
313 1999). Clinical administration of multiple-epitopes involving both the CTL and the
314 HTL epitopes are predicted here to have a greater probability of larger human
315 population coverage worldwide.
316
317 ***B Cell Epitope Prediction***
318 *Sequence-based B Cell epitope prediction.* Protein sequence-based method
319 "Bepipred Linear Epitope Prediction" was utilized to screen linear B cell epitopes
320 from eleven different SARS-CoV-2 proteins. The tool "B Cell Epitope Prediction
321 Tools" of IEDB server (http://tools.iedb.org/bcell/) was utilized. In this screening,
322 the parameters such as hydrophilicity, flexibility, accessibility, turns, exposed
323 surface, polarity and the antigenic propensity of the polypeptides is correlated
324 with its location in the protein. This allows the search for continuous epitopes
325 prediction from protein sequence. The prediction is base on the propensity scales
326 for each of the 20 amino acids. For a window size n, the i - (n-1)/2 neighboring
327 residues on each side of residue i are used to compute the score for the residue
328 i. The method "Bepipred Linear Epitope Prediction" utilized here is based on the
329 propensity scale method as well as the physiochemical properties of the given
330 antigenic sequence to screen potential epitopes (Larsen et al., 2006).
331
332 **Characterization of potential epitopes**
333 *Epitope conservation analysis.* The shortlisted CTL, HTL and B cell epitopes

334 screened from eleven SARS-CoV-2 proteins were analyzed for the conservancy
335 of their amino acid sequence by “Epitope Conservancy Analysis” tool
336 (http://tools.iedb.org/conservancy/) of IEDB. The epitope conservancy is the
337 number of protein sequences (retrieved from NCBI) that contain that particular
338 epitope. The analysis was done against their entire respective source protein
339 sequences of SARS-CoV-2 proteins retrieved from the NCBI protein database
340 (Bui et al., 2007).
341
342 *Epitope Toxicity prediction.* The tool ToxinPred
343 (http://crdd.osdd.net/raghava/toxinpred/multi_submit.php) was used to analyze
344 the toxicity of shortlisted CTL, HTL and B cell epitopes. The tool allows to identify
345 highly toxic or non-toxic short peptides. The toxicity check analysis was done by
346 the “SVM (Swiss-Prot) based” (support vector machine) method utilizing dataset
347 of 1805 sequences as positive, 3593 negative sequences from Swissprot as well
348 as an alternative dataset comprises the same 1805 positive sequences and
349 12541 negative sequences from TrEMBLE (Gupta et al., 2013).
350
351 *Overlapping residue analysis.* The overlapping residue analysis for the shortlisted
352 38 CTL, 33 HTL and the 12 B cell linear epitopes was performed by the Multiple
353 Sequence Alignment (MSA) analysis by Clustal Omega tool
354 (https://www.ebi.ac.uk/Tools/msa/clustalo/) of EBI (European Bioinformatics
355 Institute) (Sievers et al., 2011). The Clustal Omega multiple sequence alignment
356 tool virtually aligns any number of protein sequences and delivers an accurate

alignment.

Epitope selected for molecular interaction study with HLA allele and TAP transporter. Based on the overlapping residue analysis of shortlisted CTL, HTL and linear B cell epitopes few numbers of CTL and HTL epitopes were chosen for further analysis. The chosen epitopes are encircled shown in Fig.2. These epitopes were chosen based on partial or full overlapping sequence region amongst all three types of epitopes (CTL, HTL and B Cell). The chosen epitopes were further analyzed for their interactions with their respective HLA allele binders and TAP cavity interaction.

Molecular interaction analysis of selected epitopes with HLA allele and TAP transporter.

Tertiary structure modeling of HLA alleles and selected T cell epitopes. The Swiss-model was used for homology modeling of the HLA class I and II allele binders of the chosen epitopes (Arnold et al., 2006). The amino acid sequences of the HLA allele binders were retrieved from Immuno Polymorphism Database (IPD-IMGT/HLA) (https://www.ebi.ac.uk/ipd/imgt/hla/allele.html). Templates for homology modeling were chosen based on the highest amino acid sequence similarity. All the generated HLA allele models had acceptable QMEAN value (cutoff -4.0) (Supplementary table S1). The QMEAN value gives a composite quality estimate involving both global as well as local analysis of the model (Benkert et al., 2008).

The PEP-FOLD 2.0 a de novo structure prediction tool at RPBS Web Portal (https://mobyle.rpbs.univ-paris-diderot.fr/cgi-bin/portal.py#forms::PEP-FOLD) was utilized to generate tertiary structures for the chosen CTL and HTL epitopes (Shen et al., 2014).

Molecular interaction analysis of chosen CTL and HTL epitopes with HLA alleles. The PatchDock tool (http://bioinfo3d.cs.tau.ac.il/PatchDock/) was utilized for *in-silico* molecular docking study of the selected CTL and HTL epitopes with their respective HLA class I and II allele binders (Bell et al., 2005; Duhovny et al., 2002; Schneidman-Duhovny et al., 2005). PatchDock utilizes an algorithm for unbound (real- life) docking of molecules for protein-protein complex formation. The algorithm carries out the rigid docking, with the surface variability/flexibility implicitly addressed through liberal intermolecular penetration. The algorithm focuses on the (i) initial molecular surface fitting on localized, curvature-based surface patches (ii) use of Geometric Hashing and Pose Clustering for initial transformation detection (iii) computation of shape complementarity utilizing the Distance Transform (iv) efficient steric clash detection and geometric fit scoring based on a multi-resolution shape representation and (v) utilization of biological information by focusing on hot-spot rich surface patches (Bell et al., 2005; Duhovny et al., 2002; Schneidman-Duhovny et al., 2005).

Molecular interaction analysis of selected CTL epitopes with TAP transporter. TAP transporter plays an important role in the presentation of CTL epitope. From

the cytosol after proteasome processing, the fragmented peptide of foreign protein gets transported to endoplasmic reticulum (ER) through the TAP transporter. From the ER these short peptides reach to Golgi bodies and then get presented on the cell surface (Abele et al., 2004). Molecular interaction study of the chosen CTL epitopes within the TAP transporter cavity was performed by molecular docking study utilizing the PatchDock tool. For accurate prediction, the cryo-EM structure of TAP transporter (PDB ID: 5u1d) was used by removing the antigen from TAP cavity of the original structure (Oldham et al., 2016).

Design, characterization and molecular interaction analysis of Multi-Epitope Vaccines with immune receptor.

Design of Multi-Epitope Vaccines. The screened and shortlisted high scoring 38 CTL and 33 HTL epitopes were utilized to design CTL and HTL Multi-Epitope vaccines (Table 1 and 2). Short peptide EAAAK and GGGGS were used as rigid and flexible linkers respectively (Fig.2). The GGGGS linker provides proper conformational flexibility to the vaccine tertiary structure and hence facilitates stable conformation to the vaccine. The EAAAK linker facilitates in domain formation and hence facilitates the vaccine to obtain its final stable structure. Truncated (residues 10-153) Onchocerca volvulus activation-associated secreted protein-1 (Ov-ASP-1) has been utilized as an adjuvant at N terminal of both the CTL and HTL MEVs (MacDonald et al., 2005; Guo et al., 2015; He et al., 2009; Hu et al., 2004; Hajighahramani et al., 2017; Chen et al., 2013; Srivastava et al., 2019; Srivastava et al., 2018).

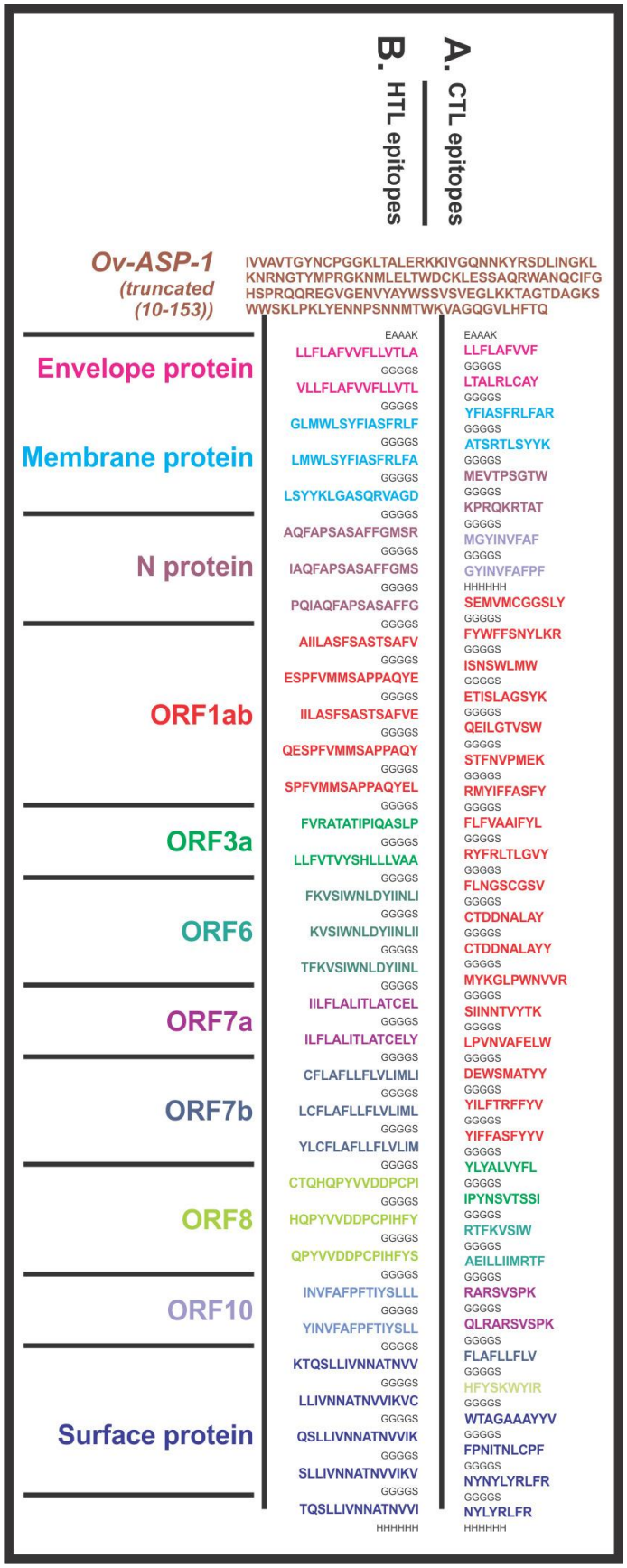

449 **Figure 2. Design of SARS-CoV-2 Multi-Epitope Vaccine (MEVs). (A)** CTL and
450 **(B)** HTL epitopes were linked by the short peptide linker 'GGGGS'. Truncated
451 (residues 10-153) Onchocerca volvulus activation-associated secreted protein-1
452 (Ov-ASP-1) has been utilized at the N terminal of both the MEVs. The short
453 peptide EAAAK was used to link Ov-ASP-1 at N terminal. Epitopes from different
454 proteins were colored in different colors. C terminal 6xHis is designed as His tag.
455
456 ***Characterization of designed Multi-Epitope Vaccines***
457 *Physicochemical property analysis of designed MEVs.* The ProtParam
458 (https://web.expasy.org/protparam/) tool was utilized to analyze the
459 physiochemical properties of the amino acid sequence of the designed CTL and
460 HTL MEVs (Gasteiger et al., 2005). The ProtParam analysis performs an
461 empirical investigation for the given query amino acid sequence. ProtParam
462 computes various physicochemical properties derived from a given protein
463 sequence.
464
465 *Interferon-gamma inducing epitope prediction.* From the designed amino acid
466 sequence of both the MEVs potential interferon-gamma (IFN-γ) epitopes were
467 screened by "IFN epitope" server
468 (http://crdd.osdd.net/raghava/ifnepitope/scan.php) using "Motif and SVM hybrid",
469 (MERCI: Motif-EmeRging and with Classes-Identification, and SVM: support
470 vector machine) method. The tool predicts peptides from protein sequences
471 having the capacity to induce IFN-gamma release from CD4+ T cells. This

472 module generates overlapping peptides from the query sequence and predicts
473 IFN-gamma inducing peptides. For the screening, IEDB database with 3705 IFN-
474 gamma inducing and 6728 non-inducing MHC class II binders are utilized
475 (Nagpal et al., 2015; Dhanda et al., 2013).
476
477 *MEVs allergenicity and antigenicity prediction.* Both the designed MEVs were
478 further analyzed for allergenicity and antigenicity prediction by utilizing the
479 AlgPred (http://crdd.osdd.net/raghava/algpred/submission.html) and the Vaxigen
480 (http://www.ddg-pharmfac.net/vaxijen/VaxiJen/VaxiJen.html) tools respectively
481 (Saha et al., 2006; Doytchinova and Flower 2007). The AlgPred prediction is
482 based on the similarity of already known epitope with any region of the submitted
483 protein. For the screening of allergenicity, the Swiss-prot dataset consisting of
484 101725 non-allergens and 323 allergens is utilized. The VaxiJen utilizes an
485 alignment-free approach, solely based on the physicochemical properties of the
486 query amino acid sequence. For the prediction of antigenicity, the Bacterial, viral
487 and the tumor protein datasets are used by VaxiJen to derive models for the
488 prediction of whole protein antigenicity. Every set consisted of known 100
489 antigens and 100 non-antigens.
490
491 *Tertiary structure modeling and refinement of MEVs.* The tertiary structure of
492 both the designed CTL and HTL MEVs were generated by homology modeling
493 utilizing the I-TASSER modeling tool (https://zhanglab.ccmb.med.umich.edu/I-
494 TASSER/). The I-TASSER is a tool for protein structure prediction based on the

sequence-to-structure-to-function paradigm (Roy et al., 2010). The tool generates three-dimensional (3D) atomic models from multiple threading alignments and iterative structural assembly simulations for a submitted amino acid sequence. I-TASSER works based on the structure templates identified by LOMETS, a meta-server, from the PDB library. I-TASSER only uses the templates of the highest Z-score which is the difference between the raw and average scores in the unit of standard deviation. For each target model, the I-TASSER simulations generate a large ensemble of structural conformations, called decoys. To select the final models, I-TASSER uses the SPICKER program to cluster all the decoys based on the pair-wise structure similarity and reports up to five models. The Normalized Z-score >1 mean a good alignment and vice versa. The Cov represents the coverage of the threading alignment and is equal to the number of aligned residues divided by the length of query protein. Ranking of templet proteins is based on TM-score of the structural alignment between the query structure model and known structures. The RMSD is the RMSD between templet residues and query residues that are structurally aligned by TM-align.

The refinement of both the generated MEV models was performed by ModRefiner (https://zhanglab.ccmb.med.umich.edu/ModRefiner/) and GalaxyRefine tool (http://galaxy.seoklab.org/cgi-bin/submit.cgi?type=REFINE) (Dong et al., 2011). TM-score generated by ModRefiner indicates the structural similarity of the refined model with the original input model. Closer the TM-Score to 1, higher would be the similarity of original and the refined model. RMSD value of the refined model shows the conformational deviation from the initial input

518 models.

519 The GalaxyRefine tool refines the query tertiary structure by repeated
520 structure perturbation as well as by utilizing the subsequent structural relaxation
521 by the molecular dynamics simulation. The tool GalaxyRefine generates reliable
522 core structures from multiple templates and then re-builds unreliable loops or
523 termini by using an optimization-based refinement method (Ko et al., 2012; Wang
524 et al., 2013; Shin et al., 2014). To avoid any breaks in the 3D model
525 GalaxyRefine uses the triaxial loop closure method. The MolProbity score
526 generated for a given refined model indicates the log-weighted combination of
527 the clash score, the percentage of Ramachandran not favored residues and the
528 percentage of bad side-chain rotamers.

529

530 *Validation of CTL and HTL MEVs refined models.* Both the refined CTL and HTL
531 MEV 3D models were further validated by RAMPAGE analysis tool
532 (http://mordred.bioc.cam.ac.uk/~rapper/rampage.php) (S.C. Lovell et al., 2008;
533 Ramakrishnan, C. et al., 1965). The generated Ramachandran plots for the MEV
534 models show the sterically allowed and disallowed residues along with their
535 dihedral psi (ψ) and phi (φ) angles.

536

537 *Linear and Discontinuous B-cell epitope prediction from MEVs.* The Ellipro
538 (ElliPro: Antibody Epitope Prediction tool; http://tools.iedb.org/ellipro/) method
539 available at IEDB, was used to screen the linear and the discontinuous B cell
540 epitopes from the MEVs vaccine models. The ElliPro method analyses based on

the location of residue in the protein's 3D structure. The residues lying outside of an ellipsoid covering 90% of the inner core protein residues score highest Protrusion Index (PI) of 0.9; and so on. The discontinuous epitopes predicted by the ElliPro tool are clustered based on the distance "R" in Å between two residue's centers of mass lying outside of the largest possible ellipsoid. The larger value of R indicates larger distant residues (residue discontinuity) are screened in the epitopes (Kringelum et al., 2012; Ponomarenko et al., 2008).

Molecular interaction analysis of MEVs with immunological receptor.

Molecular docking study of MEVs and TLR-3. Molecular interaction analysis of both the designed MEVs with Toll-Like receptor-3 (TLR-3), was performed by molecular docking and molecular dynamics simulation. Molecular docking was performed by PatchDock server (http://bioinfo3d.cs.tau.ac.il/PatchDock/) (Schneidman-Duhovny et al., 2005). PatchDock utilizes an algorithm for unbound (mimicking real- world environment) docking of molecules for protein-protein complex formation as explained earlier (Bell et al., 2005; Duhovny et al., 2002). For molecular docking, the 3D structure of human TLR-3 ectodomain (ECD) was retrieved from PDB databank (PDB ID: 2A0Z). The study provides dynamical properties of the designed system with MEVs-TLR3 complexes with a guess at the interactions between the molecules, and also it gives 'exact' predictions of bulk properties including the hydrogen bond formation and conformation of the molecules forming the complex.

Molecular Dynamics (MD) Simulations study of MEVs and TLR-3 complex. The

MEVs-TLR3 molecular interactions were further evaluated using molecular dynamics simulations analysis. MD simulation studies were performed for 10 ns by using YASARA (Yet Another Scientifc Artifcial Reality Application) (Krieger, E. and Vriend, G., et al., 2015).The simulations were carried out in an explicit water environment in a dodecahedron simulation box at a constant temperature (298K) and pressure (1 atm) and pH 7.4 with periodic cell boundary condition. The solvated systems were neutralized with counter ions (NaCl) (conc. 0.9 M). The AMBER14 force field have been applied on to the systems during simulation (Maier, J.A., et al., 2015; Case, D.A., et al., 2014). Long-range electrostatic energy and forces were calculated using particle-mesh-based Ewald method (Toukmaji, A., et al., 2000). The solvated structures was minimized by the steepest descent method at a temperature of 298K and a constant pressure. Then the complexes were equilibrated for a 1ns period. After equilibration, a production MD was run for 10 ns at a constant temperature and pressure and time frames were saved at every 10 ps for each simulation. The RMSD and RMSF values for Cα, Back bone and all the atoms of both the MEV complexes were analyzed for each simulation conducted.

In-silico analysis of MEVs for cloning and expression potency

Analysis of cDNA of both the MEVs for cloning and expression in the mammalian host cell line. Complementary DNA of both the MEVs, codon-optimized for expression in Mammalian cell line (Human) was generated by Java Codon Adaptation Tool (http://www.jcat.de/). The generated cDNA of both the MEVs

was further analyzed by GenScript Rare Codon Analysis Tool (https://www.genscript.com/tools/rare-codon-analysis). The tool analyses the GC content, Codon Adaptation Index (CAI) and the Tandem rare codon frequency for a given cDNA (Morla et al., 2016; Wu et al., 2010). The CAI indicates the possibility of cDNA expression in a chosen expression system. The tandem rare codon frequency indicates the presence of low-frequency codons in the given cDNA.

RESULTS & DISCUSSION

Screening of potential epitopes

T cell Epitope Prediction

Screening of Cytotoxic T lymphocyte (CTL) Epitope. Cytotoxic T lymphocyte (CTL) epitopes were screened by “MHC-I Binding Predictions” and “MHC-I Binding Predictions” IEDB tools. These epitopes are shortlisted based on the total amount of cleavage site in the protein, low IC(50) (nM) value for epitope-HLA class I allele pairs, and for binding to TAP cavity.

The 38 epitopes predicted by “MHC-I Binding Predictions” tool with the highest “Percentile Rank” were shortlisted for multi-epitope vaccine design and are listed in table 1. Rest 101 epitopes-HLA I allele pairs are listed in Supplementary table S8. The 67 epitopes-HLA I allele pairs predicted by “MHC-I Processing Predictions” tool with the highest “Total score” are listed in Supplementary table 9.

The immunogenicity of the shortlisted CTL epitopes was also determined and are mentioned in table 1, Supplementary table S8, and S9. The higher immunogenicity score indicates the greater immunogenic potential of the given epitope.

Table 1. Shortlisted high percentile ranking SARS-CoV-2 CTL epitopes. Selected high percentile CTL epitopes and their respective HLA alleles binders are listed. *In-silico* analysis has shown all the selected epitopes to be non-toxic (Non-Toxin) as well as they show significant conservancy and high immunogenicity. Six epitopes shown with ** show exact match with the epitopes published by Grifoni et al., 2020, indicate consensus in results.

SARS-CoV-2 Proteins	S.No	Peptide	Conservancy	Immunogenicity	Toxicity	Allele	Length	Method used	Percentile Rank
E Protein	1	LLFLAFVVF	99.59% (480/482)	0.2341	Non-Toxin	B*15:01	9	Consensus (ann/comblib_sidney2008/smm)	0.1
E Protein	2	LTALRLCAY	99.17% (478/482)	0.01886	Non-Toxin	A*01:01	9	Consensus (ann/smm)	0.12
M Protein	3	YFIASFRLFAR	99.37% (474/477)	0.19709	Non-Toxin	A*33:01	11	ann	0.03
M Protein	4	ATSRTLSYYK**	98.95% (472/477)	-0.13563	Non-Toxin	A*11:01	10	Consensus (ann/smm)	0.06
N protein	5	MEVTPSGTW	97.39% (485/498)	-0.06279	Non-Toxin	B*44:02	9	Consensus (ann/smm)	0.06
N protein	6	KPRQKRTAT	97.79% (487/498)	-0.20542	Non-Toxin	B*07:02	9	Consensus (ann/comblib_sidney2008/smm)	0.1
orf10	7	MGYINVFAF	99.38% (477/480)	-0.09452	Non-Toxin	B*35:01	9	Consensus (ann/comblib_sidney2008/smm)	0.1
orf10	8	GYINVFAFPF**	98.31% (232/236)	0.20158	Non-Toxin	A*23:01	10	Consensus (ann/smm)	0.11
orf-1ab	9	SEMVMCGGSLY	99.12% (452/456)	0.32633	Non-Toxin	B*44:02	11	ann	0.03
orf-1ab	10	FYWFFSNYLKR	99.78% (455/456)	0.37766	Non-Toxin	A*33:01	11	ann	0.04
orf-1ab	11	ISNSWLMW	99.56% (454/456)	-0.24791	Non-Toxin	B*58:01	8	ann	0.05
orf-1ab	12	ETISLAGSYK	99.78% (455/456)	0.08174	Non-Toxin	A*68:01	10	Consensus (ann/smm)	0.06
orf-1ab	13	QEILGTVSW	99.78% (455/456)	0.27341	Non-Toxin	B*44:02	9	Consensus (ann/smm)	0.06
orf-1ab	14	STFNVPMEK	100% (456/456)	-0.32016	Non-Toxin	A*11:01	9	Consensus (ann/smm)	0.06
orf-1ab	15	RMYIFFASFY	100% (456/456)	0.21107	Non-Toxin	A*30:02	10	Consensus (ann/smm)	0.06
orf-1ab	16	FLFVAAIFYL	99.56% (454/456)	-0.19814	Non-Toxin	A*02:01	10	Consensus (ann/smm)	0.06
orf-1ab	17	RYFRLTLGVY	100% (456/456)	0.03976	Non-Toxin	A*30:02	10	Consensus (ann/smm)	0.06
orf-1ab	18	FLNGSCGSV	100% (456/456)	-0.20585	Non-Toxin	A*02:03	9	Consensus (ann/smm)	0.06
orf-1ab	19	CTDDNALAY	99.37% (476/479)	0.32004	Non-Toxin	A*01:01	9	Consensus (ann/smm)	0.06
orf-1ab	20	CTDDNALAYY**	99.37% (476/479)	0.28694	Non-Toxin	A*01:01	10	Consensus (ann/smm)	0.06
orf-1ab	21	MYKGLPWNVVR	100% (456/456)	-0.11151	Non-Toxin	A*33:01	11	ann	0.06
orf-1ab	22	SIINNTVYTK**	100% (456/456)	0.15936	Non-Toxin	A*11:01	10	Consensus (ann/smm)	0.06
orf-1ab	23	LPVNVAFELW	98.68% (450/456)	-0.00254	Non-Toxin	B*53:01	10	Consensus (ann/smm)	0.06
orf-1ab	24	DEWSMATYY**	99.78% (455/456)	0.07355	Non-Toxin	B*44:03	9	Consensus (ann/smm)	0.07
orf-1ab	25	YILFTRFFYV	99.56% (454/456)	-0.02845	Non-Toxin	A*02:06	10	Consensus (ann/smm)	0.07
orf-1ab	26	YIFFASFYYV	100% (456/456)	0.12661	Non-Toxin	A*02:06	10	Consensus (ann/smm)	0.07
ORF3a	27	YLYALVYFL**	100% (456/456)	0.40924	Non-Toxin	A*02:01	9	Consensus (ann/comblib_sidney2008/smm)	0.1
ORF3a	28	IPYNSVTSSI	99.56% (454/456)	0.13772	Non-Toxin	B*51:01	10	Consensus (ann/smm)	0.11
Orf6	29	RTFKVSIW	96.88% 466/481	0.13151	Non-Toxin	B*57:01	8	ann	0.05
Orf6	30	AEILLIIMRTF	97.92% 471/481	-0.32835	Non-Toxin	B*44:02	11	ann	0.06
ORF7a	31	RARSVSPK	99.79% (480/481)	-0.18221	Non-Toxin	A*30:01	8	ann	0.11
ORF7a	32	QLRARSVSPK	99.58% (479/481)	0.1815	Non-Toxin	A*03:01	10	Consensus (ann/smm)	0.16
orf7b	33	FLAFLLFLV	98.33% (472/480)	-0.16177	Non-Toxin	A*02:03	9	Consensus (ann/smm)	0.07

orf8	34	HFYSKWYIR	98.33% (472/480)	-0.27456	Non-Toxin	A*31:01	9	Consensus (ann/smm)	0.11
S Protein	35	WTAGAAAYYV	99.58% (470/472)	0.15455	Non-Toxin	A*68:02	10	Consensus (ann/smm)	0.06
S Protein	36	FPNITNLCPF	100.00% (472/472)	0.1009	Non-Toxin	B*53:01	10	Consensus (ann/smm)	0.06
S Protein	37	NYNYLYRLFR	98.52% (465/472)	0.08754	Non-Toxin	A*33:01	10	Consensus (ann/smm)	0.07
S Protein	38	NYLYRLFR	98.52% (465/472)	0.13144	Non-Toxin	A*33:01	8	ann	0.07

Screening of Helper T lymphocyte (HTL) epitopes. The screening of helper T lymphocyte (HTL) epitopes from eleven different proteins of SARS-CoV-2 was performed based on "Percentile rank". The smaller the value of percentile rank the higher would be the affinity of the peptide with its respective HLA allele binders. The 33 epitopes with high percentile ranking were shortlisted (Table 2). Another 180 potential HTL cell epitopes-HLA allele II pairs with high Percentile rank, screened in our study are listed in Supplementary table S10.

Table 2. Shortlisted high scoring SARS-CoV-2 HTL epitopes. Selected high scoring HTL epitopes and their respective HLA alleles binders are listed. *In-silico* analysis has shown all the selected epitopes to be non-toxic (Non-Toxin) as well as they show significant conservancy. Four epitopes shown with ** show exact match with the epitopes published by Grifoni et al., 2020, indicate consensus in results.

SARS-CoV-2 Proteins	S.No.	Peptide	Conservancy	Non-Toxin	Allele	Method used	Percentile Rank
E Protein	1	LLFLAFVVFLLVTLA	99.59% (480/482)	Non-Toxin	DPA1*03:01/DPB1*04:02	Consensus (comb.lib./smm/nn)	0.02
E Protein	2	VLLFLAFVVFLLVTL	99.59% (480/482)	Non-Toxin	DPA1*03:01/DPB1*04:02	Consensus (comb.lib./smm/nn)	0.02
M Protein	3	GLMWLSYFIASFRLF	97.48% (465/477)	Non-Toxin	DPA1*01:03/DPB1*02:01	Consensus (comb.lib./smm/nn)	0.05
M Protein	4	LMWLSYFIASFRLFA	97.69% (466/477)	Non-Toxin	DPA1*01:03/DPB1*02:01	Consensus (comb.lib./smm/nn)	0.05
M Protein	5	LSYYKLGASQRVAGD**	98.95% (472/477)	Non-Toxin	DRB1*09:01	Consensus (comb.lib./smm/nn)	0.06
N Protein	6	AQFAPSASAFFGMSR	97.59% (486/498)	Non-Toxin	DRB1*09:01	Consensus (comb.lib./smm/nn)	0.01
N Protein	7	IAQFAPSASAFFGMS	97.39% (485/498)	Non-Toxin	DRB1*09:01	Consensus (comb.lib./smm/nn)	0.01
N Protein	8	PQIAQFAPSASAFFG	97.39% (485/498)	Non-Toxin	DRB1*09:01	Consensus (comb.lib./smm/nn)	0.01
ORF1ab	9	AIILASFSASTSAFV	100% (456/456)	Non-Toxin	DRB1*09:01	Consensus (comb.lib./smm/nn)	0.01
ORF1ab	10	ESPFVMMSAPPAQYE**	100% (456/456)	Non-Toxin	DRB1*01:01	Consensus (comb.lib./smm/nn)	0.01
ORF1ab	11	IILASFSASTSAFVE	100% (456/456)	Non-Toxin	DRB1*09:01	Consensus (comb.lib./smm/nn)	0.01
ORF1ab	12	QESPFVMMSAPPAQY	100% (456/456)	Non-Toxin	DRB1*01:01	Consensus (comb.lib./smm/nn)	0.01
ORF1ab	13	SPFVMMSAPPAQYEL	100% (456/456)	Non-Toxin	DRB1*01:01	Consensus (comb.lib./smm/nn)	0.01

ORF3a	14	FVRATATIPIQASLP	99.37% (478/481)	Non-Toxin	DPA1*02:01/DPB1*14:01	NetMHCIIpan	0.12
ORF3a	15	LLFVTVYSHLLLVAA	97.08% (467/481)	Non-Toxin	DRB1*01:01	Consensus (comb.lib./smm/nn)	0.1
ORF6	16	FKVSIWNLDYIINLI	99.38% (478/481)	Non-Toxin	DQA1*01:01/DQB1*05:01	Consensus (comb.lib./smm/nn)	0.02
ORF6	17	KVSIWNLDYIINLII	99.38% (478/481)	Non-Toxin	DQA1*01:01/DQB1*05:01	Consensus (comb.lib./smm/nn)	0.02
ORF6	18	TFKVSIWNLDYIINL**	99.38% (478/481)	Non-Toxin	DQA1*01:01/DQB1*05:01	Consensus (comb.lib./smm/nn)	0.02
ORF7a	19	IILFLALITLATCEL	99.79% (479/480)	Non-Toxin	DRB1*01:01	Consensus (comb.lib./smm/nn)	0.16
ORF7a	20	ILFLALITLATCELY	99.79% (479/480)	Non-Toxin	DRB1*01:01	Consensus (comb.lib./smm/nn)	0.16
ORF7b	21	CFLAFLLFLVLIMLI	97.88% (231/236)	Non-Toxin	DPA1*03:01/DPB1*04:02	Consensus (comb.lib./smm/nn)	0.03
ORF7b	22	LCFLAFLLFLVLIML	97.88% (231/236)	Non-Toxin	DPA1*03:01/DPB1*04:02	Consensus (comb.lib./smm/nn)	0.02
ORF7b	23	YLCFLAFLLFLVLIM	97.88% (231/236)	Non-Toxin	DPA1*03:01/DPB1*04:02	Consensus (comb.lib./smm/nn)	0.02
ORF8	24	CTQHQPYVVDDPCPI	99.17% (476/480)	Non-Toxin	DRB3*01:01	Consensus (comb.lib./smm/nn)	0.08
ORF8	25	HQPYVVDDPCPIHFY	99.17% (476/480)	Non-Toxin	DRB3*01:01	Consensus (comb.lib./smm/nn)	0.08
ORF8	26	QPYVVDDPCPIHFYS	99.17% (476/480)	Non-Toxin	DRB3*01:01	Consensus (comb.lib./smm/nn)	0.07
ORF10	27	INVFAFPFTIYSLLL	99.17% (476/480)	Non-Toxin	HLA-DPA1*01:03/DPB1*02:01	Consensus (comb.lib./smm/nn)	0.29
ORF10	28	YINVFAFPFTIYSLL	99.37% (476/479)	Non-Toxin	DPA1*01:03/DPB1*02:01	Consensus (comb.lib./smm/nn)	0.29
S protein	29	KTQSLLIVNNATNVV	100% (472/472)	Non-Toxin	DRB1*13:02	Consensus (smm/nn/sturniolo)	0.01
S protein	30	LLIVNNATNVVIKVC	99.36% (469/472)	Non-Toxin	DRB1*13:02	Consensus (smm/nn/sturniolo)	0.01
S protein	31	QSLLIVNNATNVVIK	99.79% (471/472)	Non-Toxin	DRB1*13:02	Consensus (smm/nn/sturniolo)	0.01
S protein	32	SLLIVNNATNVVIKV**	99.79% (471/472)	Non-Toxin	DRB1*13:02	Consensus (smm/nn/sturniolo)	0.01
S protein	33	TQSLLIVNNATNVVI	99.79% (471/472)	Non-Toxin	DRB1*13:02	Consensus (smm/nn/sturniolo)	0.01

Population Coverage by CTL and HTL epitopes. The population coverage by the shortlisted epitopes was also studied, in particular involving China, France, Italy, United States of America, South Asia, East Asia, Northeast Asia, and the Middle East. From this study, we may conclude that the combined use of all the shortlisted CTL and HTL epitopes would have an average worldwide population coverage as high as 96.10%, with a standard deviation of 23.74 (Table 3).

Table 3. World population coverage by the shortlisted SARS-CoV-2 CTL and HTL epitopes combined. With a standard deviation of 23.74 on an average 96.10 % of the world population could be covered by the joint administration of selected CTL and HTL epitopes (given in Table 1 and 2) as vaccine candidates.

654
655 a projected population coverage
656 b average number of epitope hits / HLA combinations recognized by the population
657 c minimum number of epitope hits / HLA combinations recognized by 90% of the population
658
659

Population/area	Class I and II combined		
	% coverage[a]	average_hit[b]	pc90[c]
Algeria	27.85%	1.51	0.69
American Samoa	70.35%	1.93	0.34
Argentina	96.78%	3.56	1.35
Australia	79.62%	2.73	0.49
Austria	99.28%	7.17	2.74
Belgium	97.21%	4.63	1.71
Bolivia	35.81%	2.14	0.77
Brazil	92.28%	3.69	1.15
Bulgaria	95.49%	4.48	1.64
Burkina Faso	61.26%	1.3	0.26
Cameroon	88.90%	2.71	0.9
Cape Verde	98.02%	5.71	2.07
Central Africa	87.66%	3.35	0.81
Central African Republic	36.40%	1.25	0.16
Chile	90.76%	4.36	1.06
China	90.43%	4.74	1.05
Colombia	24.90%	1.18	0.27
Congo	29.65%	1.58	0.64
Cook Islands	22.52%	1.33	0.65
Croatia	97.46%	5.28	1.97
Cuba	97.36%	6.08	2.03
Czech Republic	98.68%	5.99	2.31
Denmark	59.30%	3.61	1.23
East Africa	90.29%	3.46	1.02
East Asia	93.23%	5.49	1.29
England	99.45%	7.37	3.14
Equatorial Guinea	15.47%	0.81	0.58
Ethiopia	34.14%	1.72	0.71
Europe	98.35%	6.12	2.32
Finland	99.58%	5.27	2.46
France	98.20%	6.39	2.31
Georgia	93.92%	4.08	1.31
Germany	99.34%	7.17	2.92
Greece	26.34%	1.51	0.68
Guinea-Bissau	95.03%	4.49	1.37
Hong Kong	84.82%	2.7	0.66
India	86.82%	3.86	0.76
Indonesia	78.44%	2.93	0.46
Iran	94.14%	4.47	1.45
Ireland Northern	99.55%	7.7	3.3

Ireland South	99.28%	7.31	3.16
Israel	84.33%	3.49	0.64
Italy	96.70%	4.11	1.74
Ivory Coast	65.09%	1.16	0.29
Japan	92.78%	5.3	1.23
Jordan	85.10%	3.54	0.67
Kenya	86.65%	2.27	0.75
Korea; South	95.79%	6.18	1.72
Macedonia	43.69%	2.18	0.18
Malaysia	80.94%	3.79	0.52
Mali	95.75%	2.67	1.3
Martinique	43.47%	1.8	0.18
Mexico	93.68%	3.6	1.35
Mongolia	87.03%	4.25	0.77
Morocco	97.32%	5.55	2.01
Netherlands	40.49%	2.35	0.84
New Caledonia	61.85%	2.73	0.26
New Zealand	24.11%	1.39	0.66
Niue	20.26%	1.2	0.63
North Africa	94.14%	4.19	1.3
North America	97.36%	6	2.09
Northeast Asia	90.30%	4.71	1.04
Norway	52.39%	3.08	1.05
Oceania	75.64%	3.29	0.41
Oman	94.27%	3.2	1.35
Pakistan	85.00%	2.54	0.67
Papua New Guinea	71.23%	3.29	0.35
Peru	95.12%	3.38	1.52
Philippines	67.23%	1.92	0.61
Poland	98.46%	6.18	2.36
Portugal	96.27%	5.25	1.75
Romania	95.90%	3.54	1.56
Russia	94.88%	5.26	1.49
Rwanda	45.12%	1.85	0.18
Samoa	43.64%	2.65	0.89
Sao Tome and Principe	96.32%	4.15	1.54
Saudi Arabia	96.53%	4.87	1.65
Scotland	73.06%	4.19	0.37
Senegal	94.11%	3.54	1.24
Serbia	62.91%	1.07	0.27
Singapore	86.92%	4.37	0.76
Slovenia	43.37%	2.58	0.88
South Africa	88.81%	2.6	0.89
South America	81.68%	2.95	0.55
South Asia	90.37%	4.25	1.03
Southeast Asia	82.33%	3.79	0.57

Southwest Asia	86.38%	3.13	0.73
Spain	87.57%	3.8	0.8
Sri Lanka	52.39%	1.59	0.42
Sudan	87.98%	2.69	0.83
Sweden	99.29%	7.32	2.59
Taiwan	84.93%	4.28	0.66
Thailand	91.26%	4.81	1.17
Tonga	33.43%	1.98	0.69
Tunisia	94.64%	4.17	1.38
Turkey	61.05%	2.54	0.51
Uganda	92.00%	2.99	1.13
United States	97.45%	6.04	2.11
Venezuela	69.56%	1.16	0.33
Vietnam	86.19%	4.11	0.72
West Africa	94.34%	4.44	1.32
West Indies	96.71%	5.04	1.74
Zambia	97.50%	3.1	1.67
Zimbabwe	93.60%	3.4	1.21
World	**96.10%**	**5.55**	**1.8**
Average	**78.62**	**3.73**	**1.16**
Standard deviation	**23.74**	**1.67**	**0.73**

B Cell epitope prediction

Sequence-based B Cell epitope prediction. To screen B cell epitopes we utilized the Bepipred Linear Epitope Prediction method. In our study, we screened 12 B cell epitopes, from eleven SARS-CoV-2 proteins, which show partial or complete overlap with shortlisted CTL and HTL epitope (Table 4). Another 206 B Cell epitope, with the epitope length of at least four amino acids and maximum 20 amino acids were screened and are listed in Supplementary table S11.

Table 4. Shortlisted SARS-CoV-2 B Cell epitopes. BepiPred Linear B Cell epitopes showing sequence overlap with CTL and HTL epitopes are shortlisted. *In-silico* analysis has shown all the selected epitopes to be non-toxic (Non-Toxin) as well as they show significant amino acid sequence conservancy.

SARS-CoV-2 Proteins	S.No	Overlapping B Cell Epitope (BepiPred method)	Conservancy	Length	Toxicity
M protein	1	KLGASQRVAGDS	98.74% (471/477)	12	Non-Toxin
N protein	2	RLNQLESKMSGKGQQQQGQTVTKKSAAEASK KPRQKRTATKA	96.99% (483/498)	42	Non-Toxin
ORF1ab	3	GTTQTACTDDNALAYYNTTK	99.78% 455/456	20	Non-Toxin
ORF3a	4	QGEIKDATPSDF	99.37% (478/481)	12	Non-Toxin
ORF3a	5	PYNSVT	97.92% (471/481)	6	Non-Toxin
ORF7a	6	LYHYQECVR	99.79% (479/480)	9	Non-Toxin
ORF7a	7	VKHVYQLRARSVSPKLFIRQEEVQEL	97.92% (470/480)	26	Non-Toxin
ORF8	8	QSCTQHQPYVVDDPCPIHFYSKW	95.83% (460/480)	23	Non-Toxin
ORF8	9	RVGARKSAP	99.17% (476/480)	9	Non-Toxin
S protein	10	TPGDSSSGWTA	99.58% (470/472)	11	Non-Toxin
S protein	11	FPNITNLCPFGEVFNATRFASVYAWNRKRISNCVA	99.58% (470/472)	35	Non-Toxin
S protein	12	NLDSKVGGNYNYLYRLFRKSNLKPFERDISTEIY QAGSTPCNGVEGFNCYFPLQSYGFQPTN	96.19% (454/472)	62	Non-Toxin

Characterization of potential epitopes

Epitope conservation analysis. Sequence conservation analysis of the screened CTL, HTL and B cell epitopes have shown highly conserved nature of the shortlisted epitopes. Both the CTL epitopes and the HTL epitope were found to be significantly conserved with their 100% amino acid sequence amongst the NCBI retrieved protein sequences of SARS-CoV-2 (CTL epitopes 96.88% to 100% conserved and HTL epitopes were 97.08% to 100% conserved (Table 1, 2 4, Supplementary table S8, S9, S10 & S11).

Epitope toxicity prediction. Toxicity analysis of all the screened CTL, HTL and B Cell epitopes was also performed. The ToxinPred study of all the shortlisted epitopes shows that they all are non-toxic in nature (Table 1, 2 4, Supplementary table S8, S9, S10 & S11).

Overlapping residue analysis. Amino acid sequence overlap analysis amongst the shortlisted CTL, HTL and B cell epitopes from eleven SARS-CoV-2 proteins was performed by the Multiple Sequence Alignment (MSA) analysis tool Clustal Omega. The analysis has shown that several epitopes of CTL, HTL and B cell were having amino acid sequences overlap. The CTL, HTL and B cell epitopes having two or more than two amino acid residues overlap are shown in Fig.2.

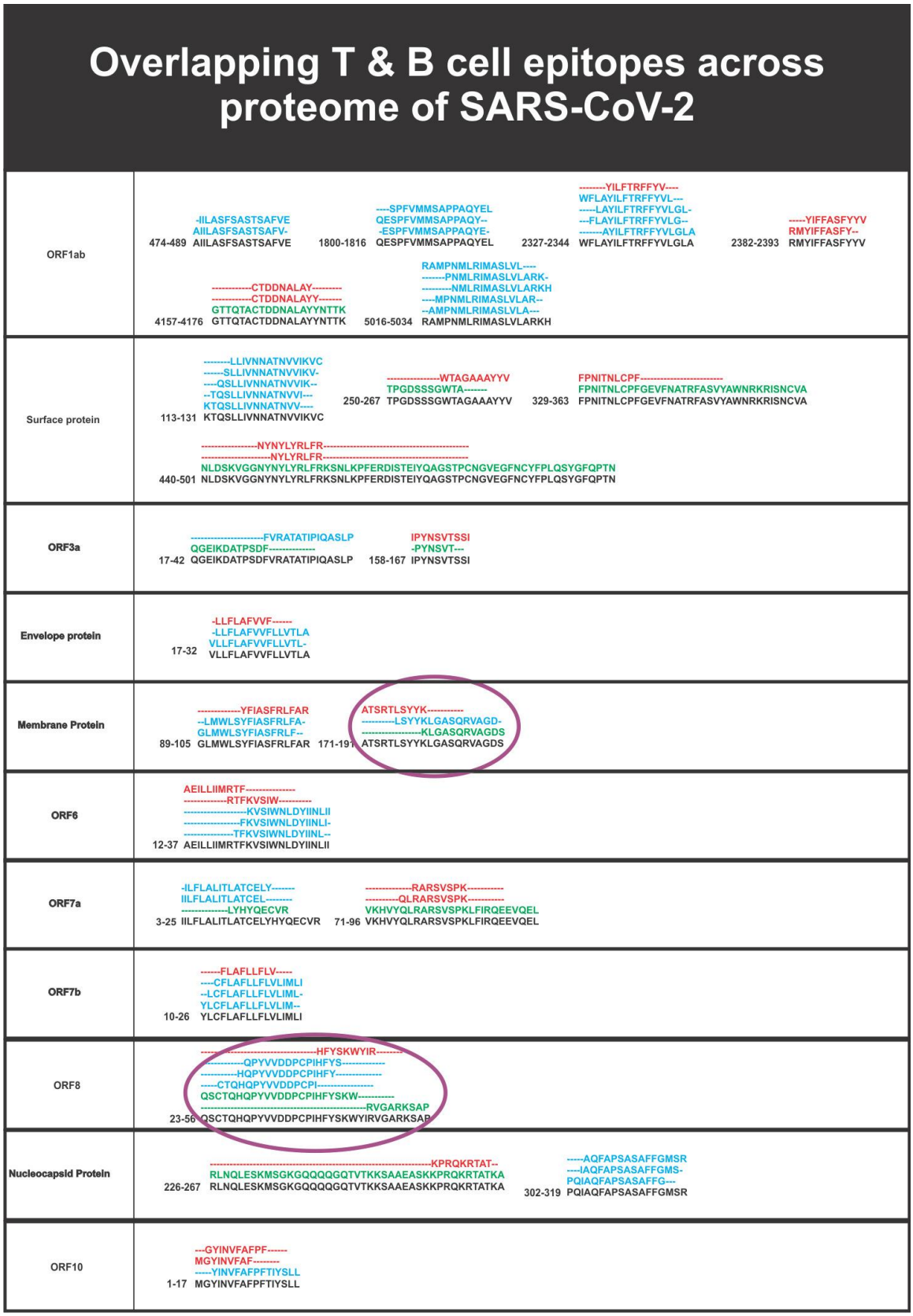

Figure 3. Overlapping SARS-CoV-2 CTL, HTL and B cell epitopes. Multiple sequence alignment performed by Clustal Omega at EBI to identify the consensus overlapping regions of CTL (red), HTL (blue) and B cell epitopes (green) amongst shortlisted epitopes. Epitopes with overlapping regions amongst all the three types of epitopes (CTL, HTL and B Cell epitopes) were chosen for further studies (encircled).

Epitope selected for molecular interaction study with HLA allele and TAP transporter. The epitopes showing overlap amongst all the three types of epitopes i.e CTL, HTL and B cell epitopes have been encircled in Fig.2 and are chosen for further study for their interaction with HLA allele and TAP (Transporter Associated with Antigen Processing) transporter.

Molecular interaction analysis of selected epitopes with HLA allele and TAP transporter.

Molecular interaction analysis of chosen CTL and HTL epitopes with HLA alleles. The molecular docking study of chosen CTL and HTL epitopes with their respective HLA class I and II allele binders was performed by PatchDock tool. The study revealed a significant molecular interaction between all the chosen epitopes and their HLA allele binders showing multiple hydrogen bond formations (Fig.3). Furthermore, the B-factor analysis of all the epitope-HLA allele complexes has also shown the epitope ligand to have stable (blue) binding conformation in complex with the HLA allele molecule (VIBGYOR color

794 presentation, blue being very stable) Fig.4.

795

796

797

798

799

800

801

802

803

804

805

806

807

808

809

810

811

812

813

814

815

816

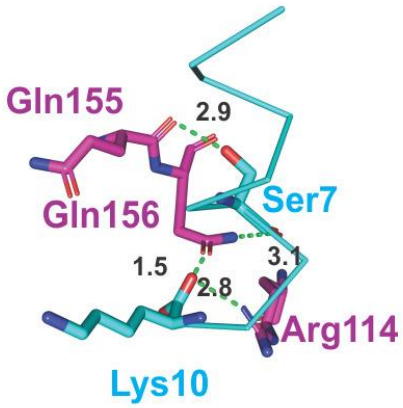

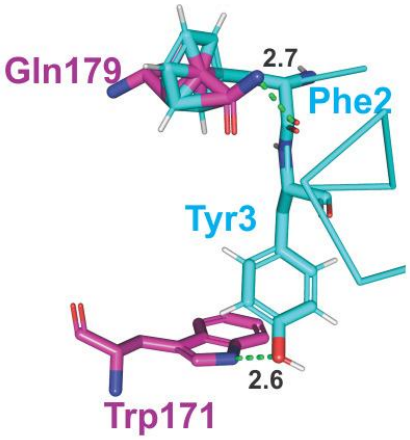

1. ATSRTLSYYK-HLA-A*11:01

2. HFYSKWYIR-HLA-A*31:01

CTL epitopes - HLA Class I allele complexes

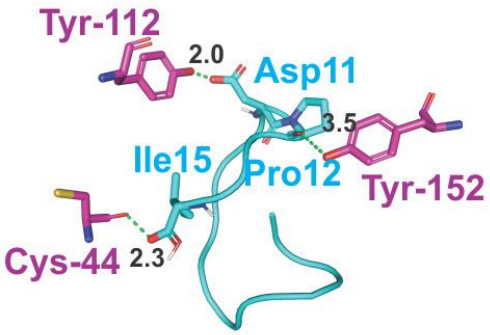

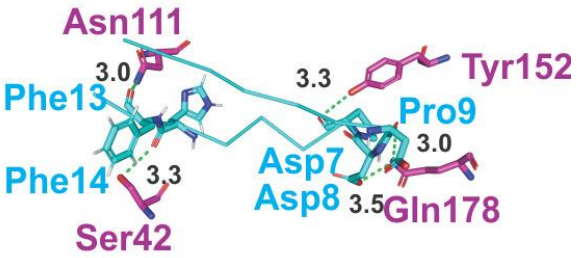

3. CTQHQPYVVDDPCPI-HLA-DRB3*01:01

4. HQPYVVDDPCPIHFY-HLA-DRB3*01:01

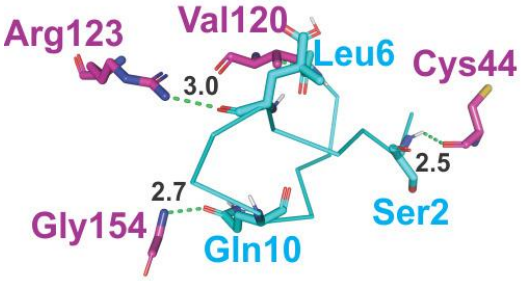

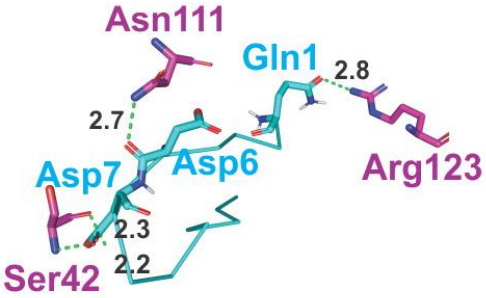

5. LSYYKLGASQRVAGD-HLA-DRB1*09:01

6. QPYVVDDPCPIHFYS-HLA-DRB3*01:01

HTL epitopes - HLA Class II allele complexes

840 **Figure 4. Molecular Docking analysis of SARS-CoV-2 CTL epitopes and**
841 **HLA alleles.** Molecular docking of chosen CTL and HTL epitopes (cyan sticks)
842 with binding amino acid residues of their respective HLA class I and class II allele
843 binders (magenta sticks). The study shows the docked complexes to form a
844 stable complex with multiple hydrogen bonds (green dots, lengths in Angstroms)
845 formation. Images were generated by the PyMOL Molecular Graphics System,
846 Version 2.0 Schrödinger, LLC.
847
848
849
850
851
852
853
854
855
856
857
858
859
860
861
862

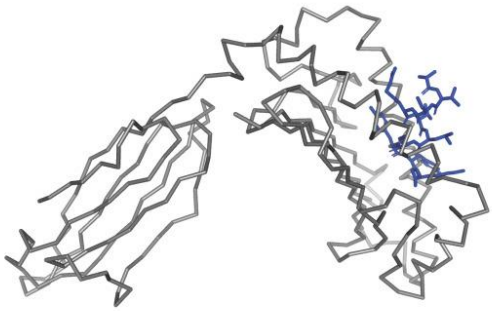

1. ATSRTLSYYK-HLA-A*11:01

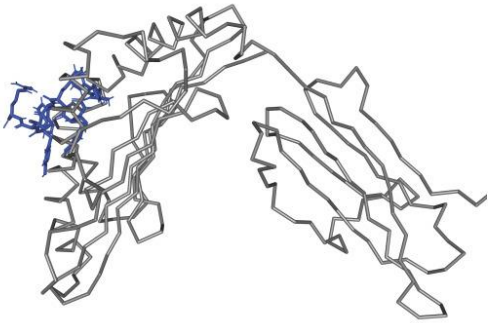

2. HFYSKWYIR-HLA-A*31:01

CTL epitopes - HLA Class I allele complexes

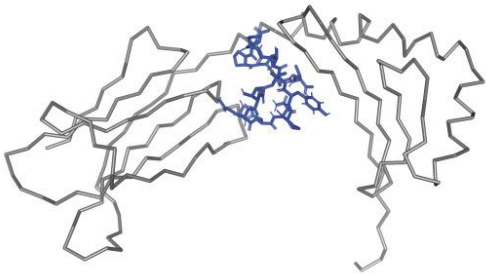

3. CTQHQPYVVDDPCPI-HLA-DRB3*01:01

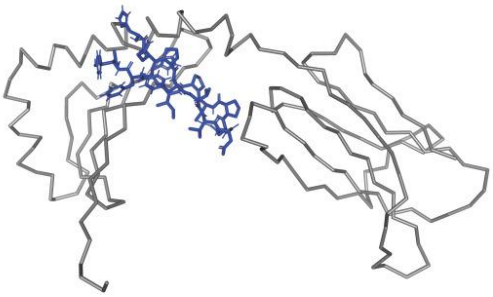

4. HQPYVVDDPCPIHFY-HLA-DRB3*01:01

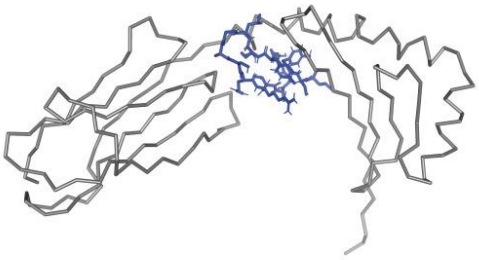

5. LSYYKLGASQRVAGD-HLA-DRB1*09:01

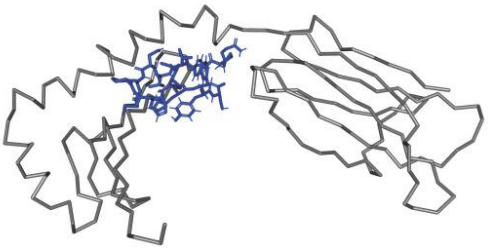

6. QPYVVDDPCPIHFYS-HLA-DRB3*01:01

HTL epitopes - HLA Class II allele complexes

886 **Figure 5. B-Factor of CTL and HTL epitope in complex with HLA class I and II**
887 **allele.** CTL and HTL Epitopes are shown in sticks and HLA Class I and II alleles are
888 shown in ribbon. The HLA alleles are shown in gray. The regions of the epitope in the
889 complex are shown in a rainbow (VIBGYOR), the regions in blue being very stable and
890 the region towards red being relatively unstable. In the complexes shown above, most of
891 the regions of epitopes are in blue indicating the complexes to be highly stable.
892
893 *Molecular interaction analysis of selected CTL epitopes with TAP transporter.*
894 The molecular docking interaction analysis of the chosen CTL epitopes with the
895 TAP transporter cavity has shown a significantly strong molecular interaction with
896 several hydrogen bonds formation at different sites of the TAP transporter cavity.
897 Two sites of interaction were of particular interest, one closer to the cytoplasmic
898 end and another closer to the ER lumen (Fig.5). This study confirms the
899 feasibility of transportation of chosen CTL epitopes from the cytoplasm to the ER
900 lumen which is an essential event for the representation of epitope by the HLA
901 allele molecules on the surface of antigen- presenting cells.
902
903
904
905
906
907
908

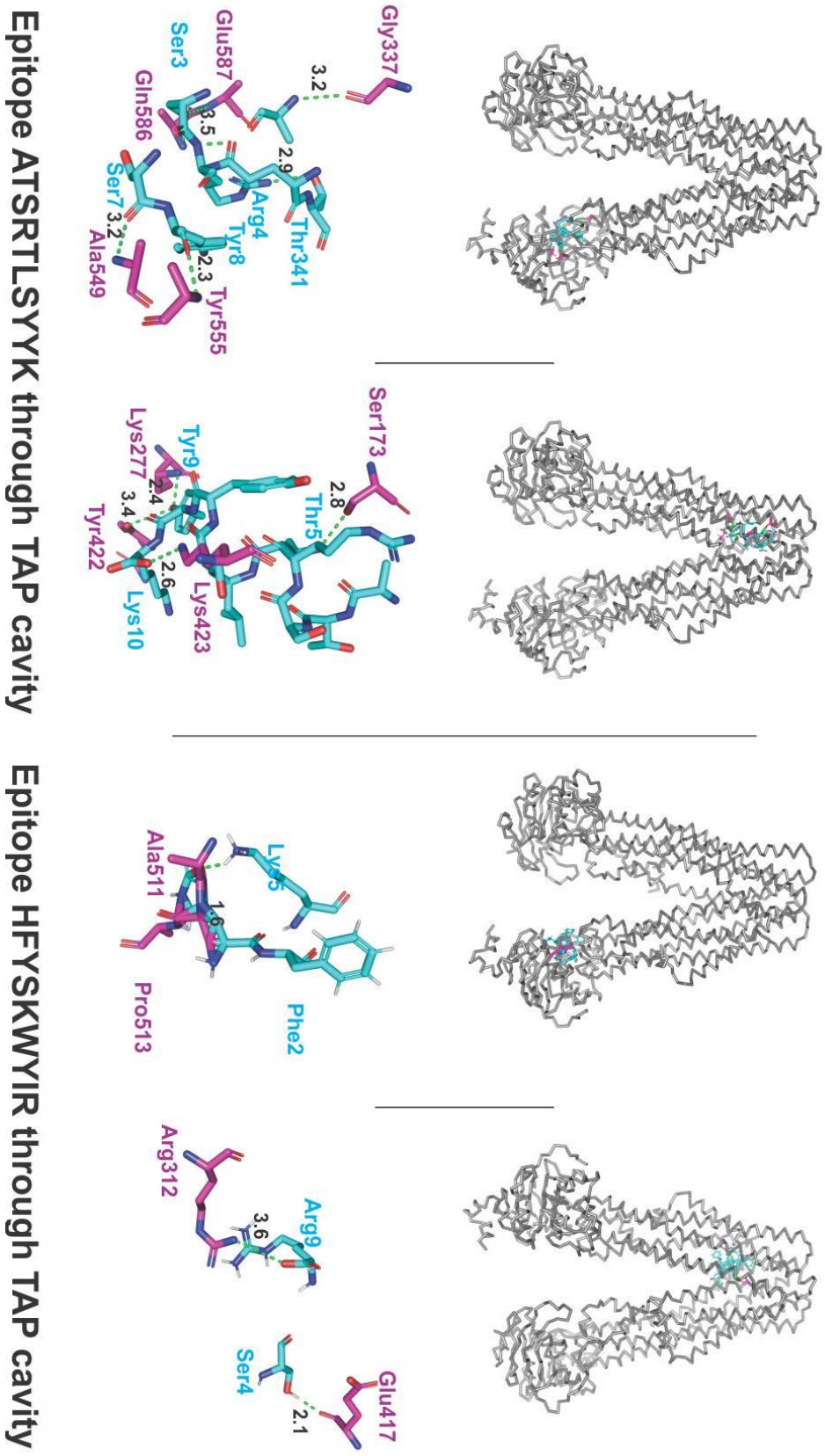

Figure 6. Molecular docking analysis of CTL epitopes within the TAP transporter cavity. Molecular interaction of CTL epitopes (cyan sticks) within the TAP cavity (gray ribbon/sticks) is shown. Detailed interaction between the residues of epitopes and TAP transporter residues have been shown with hydrogen formation shown with green dots. H bonds are shown in gereen dots with lengths in Angstroms.

Characterization and molecular interaction analysis of designed Multi-Epitope Vaccines with immune receptor

Characterization of designed Multi-Epitope Vaccines

Physicochemical property analysis of designed MEVs. ProtParam analysis for both the CTL and HTL MEVs was performed to analyze their physiochemical properties. The empirical physiochemical properties of the CTL and HTL MEVs are given in the table 5. The aliphatic index and grand average of hydropathicity (GRAVY) of both the MEVs indicate the globular and hydrophilic nature of both the MEVs. The instability index score of both the MEVs indicates the stable nature of the protein molecules (Table 5).

Table 5. Physicochemical property analysis based on amino acid sequence of designed CTL and HTL multi-epitope vaccine.

MEVs	Amino acid length	Molecular Weight	Theoretical pI	Expected half-life	Aliphatic index	Grand average of hydropathicity (GRAVY)	Instability index score
CTL MEV	704 aa	72.62 kDa	9.70	E.Coli: 10 Hr Yeast: 30 Hr Mammalian cell: 20 Hr	61.09	-0.090	44.31
HTL MEV	810 aa	82.80 kDa	8.64	Coli: 10 Hr Yeast: 30 Hr Mammalian cell: 20 Hr	96.43	0.501	40.28

Interferon-gamma inducing epitope prediction. Interferon-gamma (IFN-γ) inducing epitopes are involved in both the adaptive as well as in the innate immune response. The IFN-γ inducing 15 mer peptide epitopes were screened from the amino acid sequence of CTL and HTL MEVs by utilizing the IFNepitope server. A total of 20 CTL MEV and 20 HTL MEV INF-γ inducing POSITIVE epitopes with a score of 1 or more than 1 were shortlisted (Supplementary table S2).

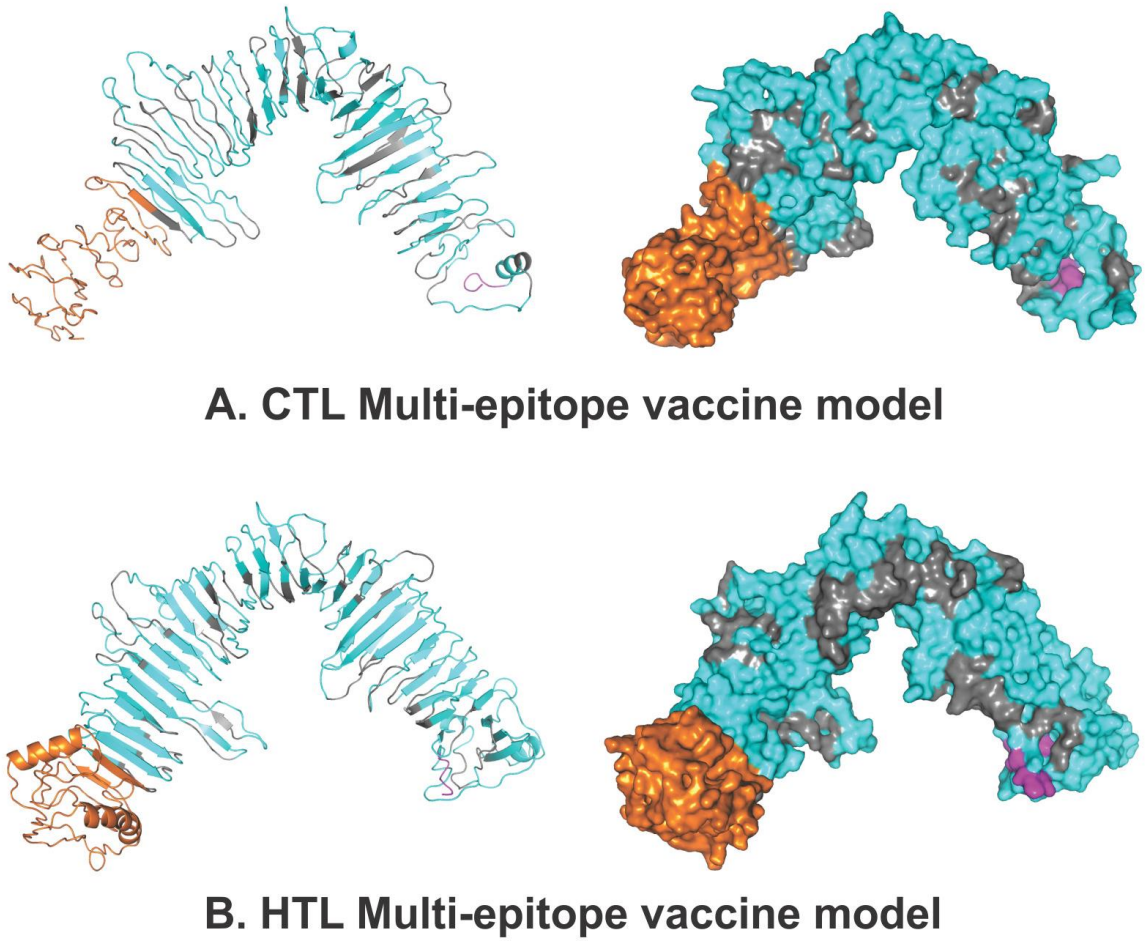

Figure 7. Tertiary structure modelling of CTL and HTL Multi-Epitope Vaccines. Tertiary structural models of CTL and HTL MEVs have been shown. The epitopes are shown in cyan. The adjuvant (Ov-ASP-1) is shown in orange. The linkers are shown in gray and 6xHis tag is shown in magenta. Both the cartoon and surface presentation of both the MEVs are shown.

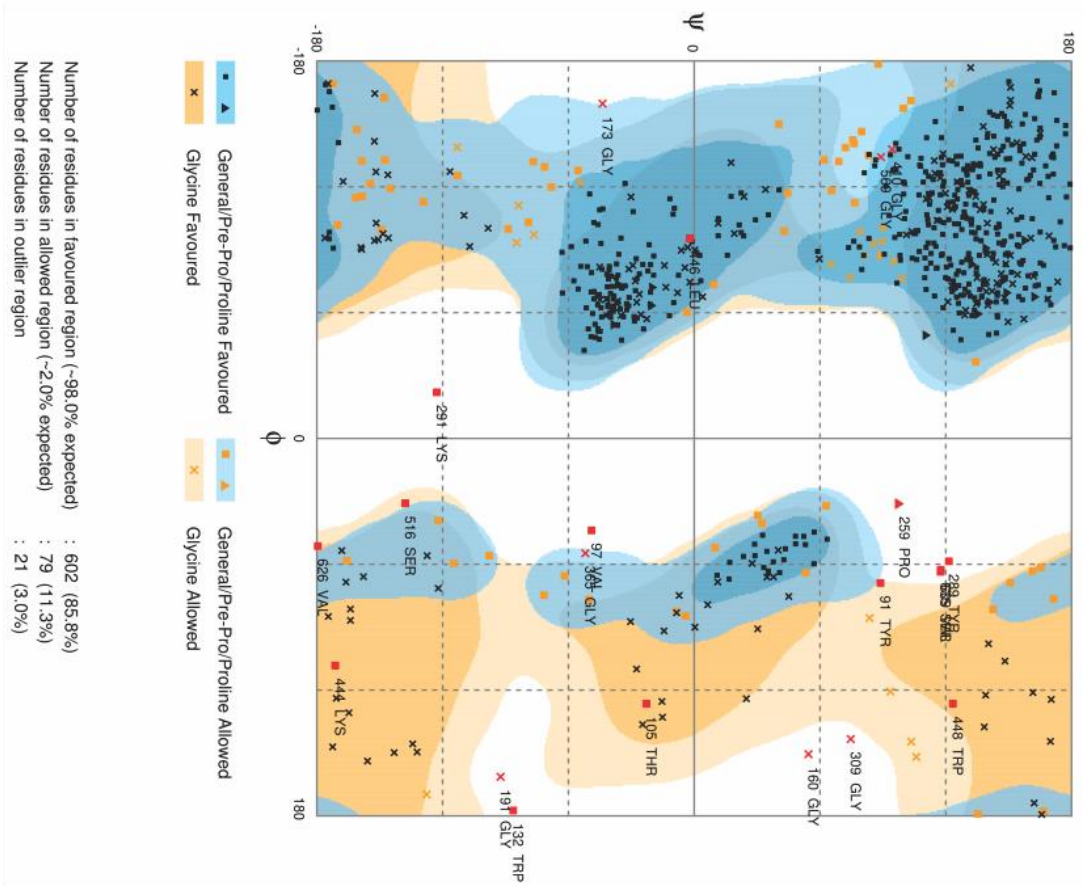

A. CTL Multi-epitope vaccine RAMPAGE analysis

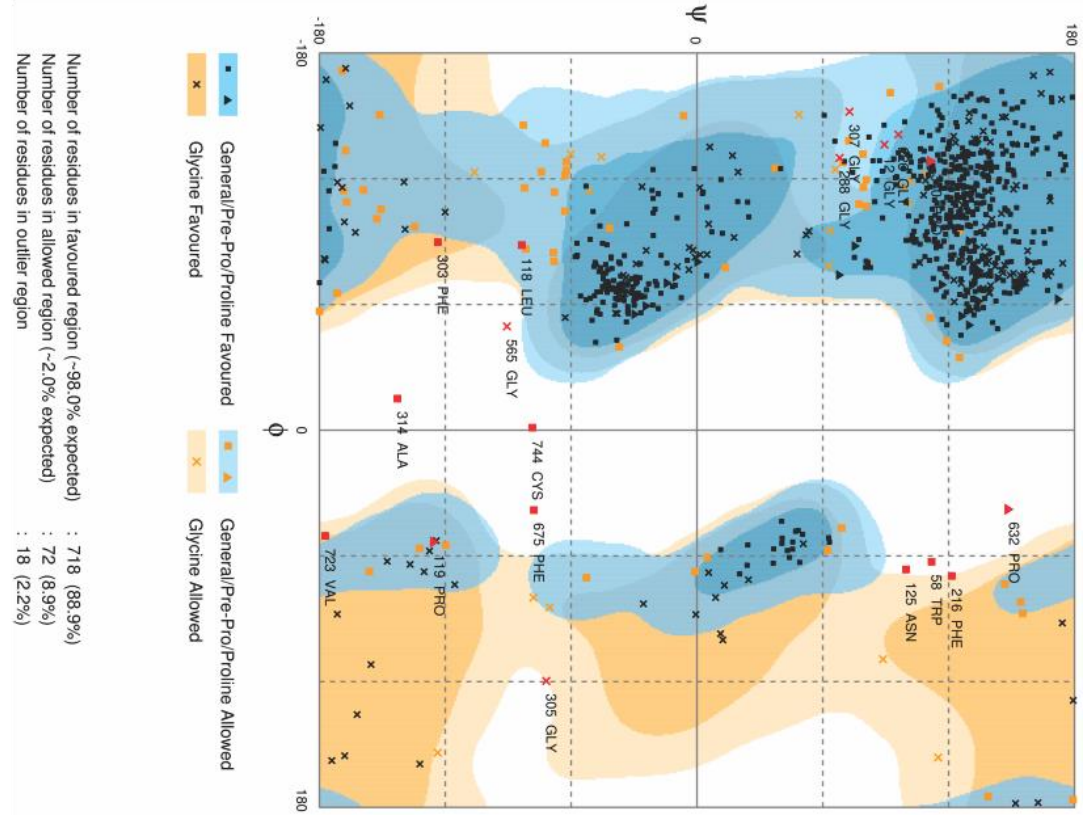

B. HTL Multi-epitope vaccine model RAMPAGE analysis

Figure 8. RAMPAGE analysis of CTL and HTL MEVs. The RAMPAGE analysis of both the CTL and HTL MEVs has been done and shown here.

MEVs allergenicity and antigenicity prediction. Both the CTL and HTL MEVs were found to be NON-ALLERGEN by the AlgPred analysis (scoring -0.95185601 and -1.1293352 respectively; threshold being -0.4). The CTL and HTL MEVs were also analyzed by VaxiJen to be probable ANTIGENS (prediction score 0.4485 and 0.4215 respectively; default threshold being 0.4). Hence with the mentioned analysis tools both the CTL and HTL MEVs are predicted to be non-allergic as well as potentially antigenic in nature.

Tertiary structure modeling and refinement of MEVs. 3D homology models were generated for both the CTL and HTL MEVs by utilizing the I-TASSER modeling tool (Fig.7). The models were generated for CTL Multi-epitope vaccine (PDB hit 5n8pA, Norm. Z-score of 1.49, Cov of 0.92, TM-score of 0.916 and RMSD of 1.04 Å) and HTL Multi-epitope vaccine (PDB hit 5n8pA, Norm. Z-score of 1.52, Cov of 0.97, TM-score of 0.916 and RMSD of 1.04 Å).

Both the generated CTL and HTL 3D models were further refined by ModRefiner to fix any gaps and then followed by GalaxyRefine refinement. The refinement by ModRefiner showed the TM-score of 0.9189 and 0.9498 for the CTL and HTL models respectively, hence being close to 1, the initial and the refined models were structurally similar. After refinement, the RMSD for CTL and HTL models with respect to the initial model was 3.367Å and 2.318Å

respectively. Further, both the CTL and HTL MEVs models were refined by GalaxyRefine and model 1 was chosen based on best scorings parameters. The CTL MEV model refinement output model (Rama favoured was 83.6%, GDT-HA was 0.9371, RMSD was 0.459, MolProbity was 2.539, Clash score was 23.2, and Poor rotamers was 1.8) and the HTL MEV model refinement output model (Rama favoured was 87.7%, GDT-HA was 0.9552, RMSD was 0.402, MolProbity was 2.537, Clash score was 27.9, and Poor rotamers was 1.6) show a well-refined and acceptable models for both of the MEVs. After refinement, all the mentioned parameters have found to be improved significantly in comparison to the initial CTL and HTL MEV models (Supplementary table S3).

Validation of CTL and HTL MEVs refined models. Both the CTL and HTL model were analyzed by the RAMPAGE analysis tool after refinement. The refined CTL MEV model was found to have 85.8% residues in favored region, 11.3% residues in allowed region, and only 3.0% residues in the outlier region; while the refined HTL MEV model was found to have 88.9% of residues in favored region, 8.9% residues in allowed region, and only 2.2% residues in the outlier region (Fig.8)

Linear and Discontinuous B-cell epitope prediction from MEVs. The linear and discontinuous B-cell epitope prediction was performed to enlist potential linear and discontinuous epitopes from the refined 3D models of CTL and HTL MEVs utilizing the ElliPro tool available on IEDB server. The screening revealed that the CTL MEV carries 17 linear and 2 potential discontinuous B cell epitopes and that

of HTL MEV carries 17 linear and 4 potential discontinuous epitopes. The high range of the PI (Protrusion Index) score of the linear and discontinuous epitopes from CTL and HTL MEVs show a high potential of the epitopes to cause humoral immune response (PI score: CTL MEV linear & discontinuous B cell epitopes - 0.511 to 0.828 & 0.664 to 0.767 respectively; HTL MEV linear and discontinuous B cell epitopes - 0.518 to 0.831 & 0.53 to 0.776 respectively) (Supplementary table S4,S5, S6, S7).

Molecular interaction analysis of MEVs with immunological receptor.

Molecular docking study of MEVs and TLR-3. Both the refined models of CTL and HTL MEVs were further studied for their molecular interaction with the ectodomain (ECD) of human TLR-3. Therefore, molecular docking of CTL and HTL MEVs model with the TLR-3 crystal structure model (PDB ID: 2A0Z) was performed utilizing the PatchDock tool. Generated docking conformation with the highest scores of 20776 and 20350 for CTL and HTL MEVs respectively were chosen for further study. The highest docking score indicates the best geometric shape complementarity fitting conformation of MEVs and the TLR-3 receptor as predicted by the PatchDock tool. Both the CTL and HTL MEVs were fitting into the ectodomain region of TLR-3 after docking (Fig.9A, 9C). The CTL and HTL MEVs have shown to form multiple hydrogen bonds within the ectodomain cavity region of TLR-3.

The B-factor analysis of MEVs-TLR3 complexes was also performed. The B-factor indicates the displacement of the atomic positions from an average

(mean) value i.e. the more flexible an atom is the larger the displacement from the mean position will be (mean-squares displacement) (Fig.9B, 9D). The B-factor analysis of the CTL and HTL MEVs bound to the TLR3 receptor shows that most of the regions of MEVs bound to TLR3 are stable nature in nature. The B-Factor analysis has been represented by the VIBGYOR color presentation with blue represents low B-factor and red represents high B-factor. Hence, the results suggest a stable complex formation tendency for both the CTL and HTL MEVs with the ectodomain of the human TLR-3 receptor (Fig.9B, 9D).

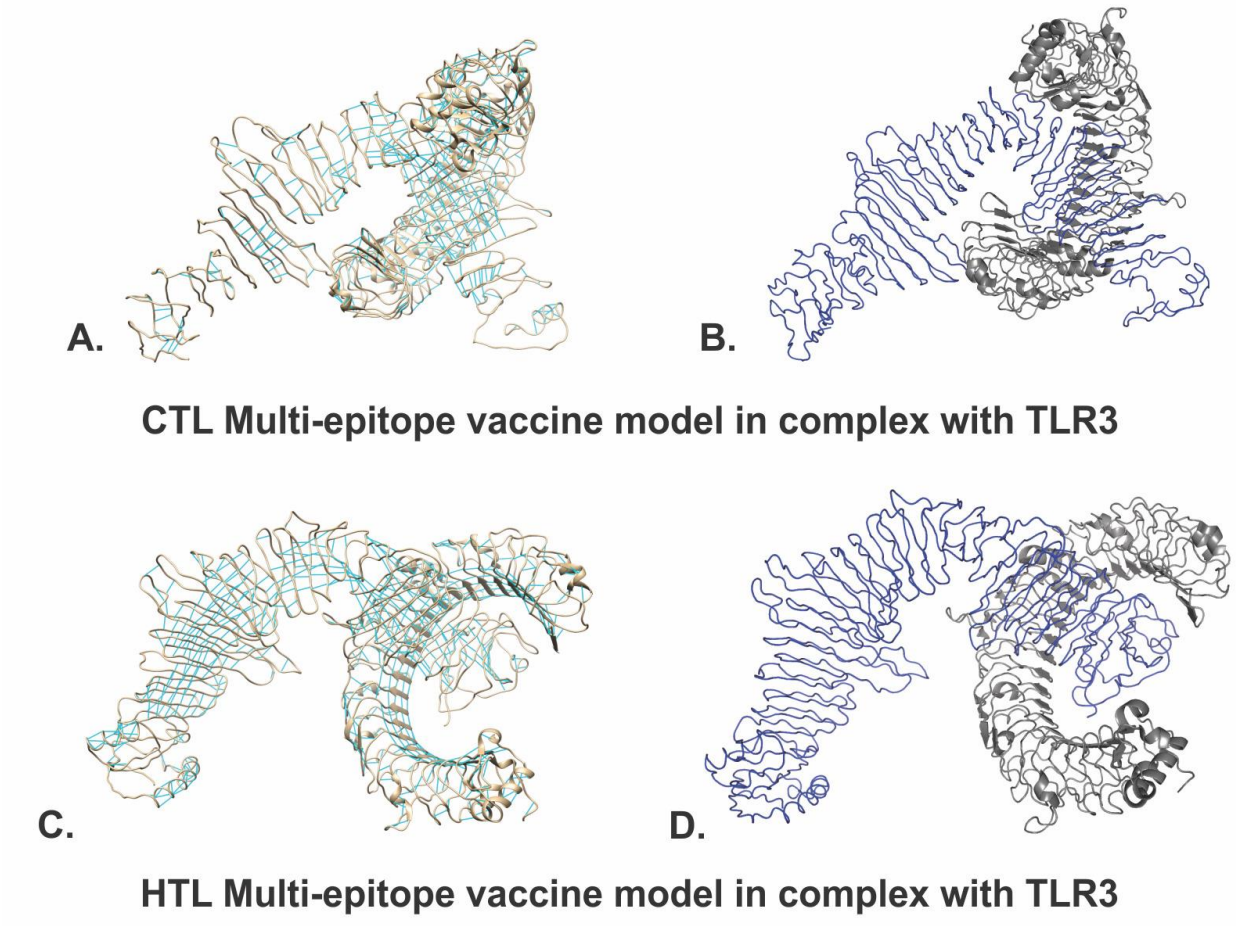

Figure 9. Molecular Docking study of CTL and HTL MEVs with TLR-3 receptor. (A), (C) The docking complex of CTL-TLR and HTL-TLR3 have been shown. The TLR3 is shown in the cartoon, and the MEVs are shown in the ribbon. Hydrogen bond formation is shown by cyan lines. **(B), (D)** B-factor presentation for the docked MEVs to the TLR3 receptor. The presentation is in VIBGYOR color, with blue showing low B-factor and red show high B-factor. Here most of the MEV regions are in blue showing low B-factor and hence indicate stable complex formation with TLR3 receptor. Images were generated by PyMol and UCSF Chimera (Pettersen et al., 2004).

Molecular Dynamics (MD) Simulations study of MEVs and TLR-3 complex. Both the complexes of CTL MEV – TLR3 and the HTL MEV – TLR3 were further subjected for molecular dynamics simulation analysis to investigate the stability of the molecular interaction involved. Both the MEVs-TLR3 complexes have shown a very convincing and reasonably stable root mean square deviation (RMSD) values for Cα , Back bone, and all atom (CTL-MEV-TLR3 Complex: ~4 to ~7.5 Å; HTL-MEV-TLR3 Complex: ~ 3.0 to ~9.8 Å) which stabilizing towards the end, Fig 10. A & C. The RMSD of both complexes was maintained to the above mentioned RMSD range for a given time window of 10 ns at reasonably invariable temperature (~278 K) and pressure (~1 atm). Molecular docking and molecular dynamics simulation study of all the MEVs-TLRs complexes indicate a stable complex formation tendency. All most all the animo acid residues of the CTL and HTL MEVs in complexed with TLR3 have shown to have root mean

square fluctuation (RMSF) in acceptable range (~2 to ~6 Å), Fig. 10 B & D. These results indicate both the CTL MEV – TLR3 and HTL MEV – TLR3 complexes to have a stable nature with acceptable molecular interaction tendency.

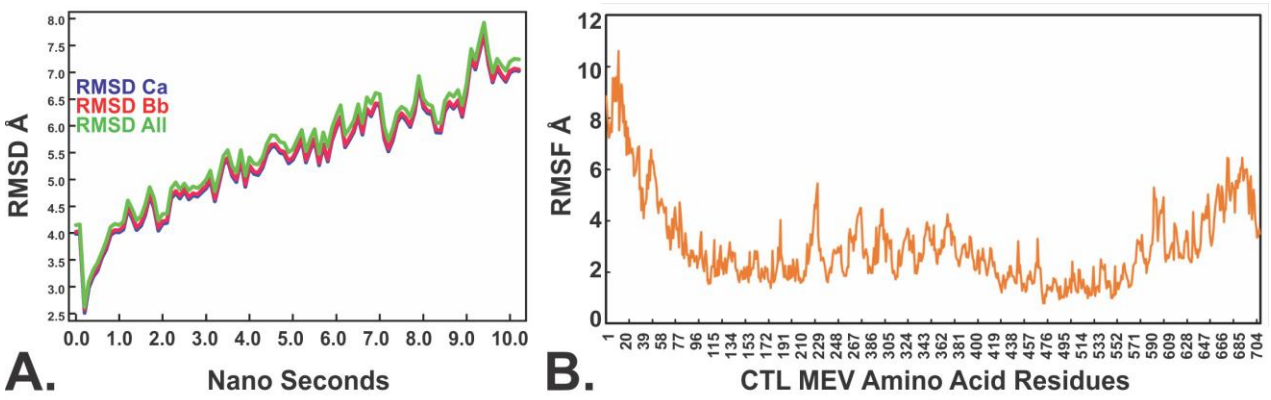

CTL Multi-epitope COVID19 vaccine - Toll Like Receptor 3 complex

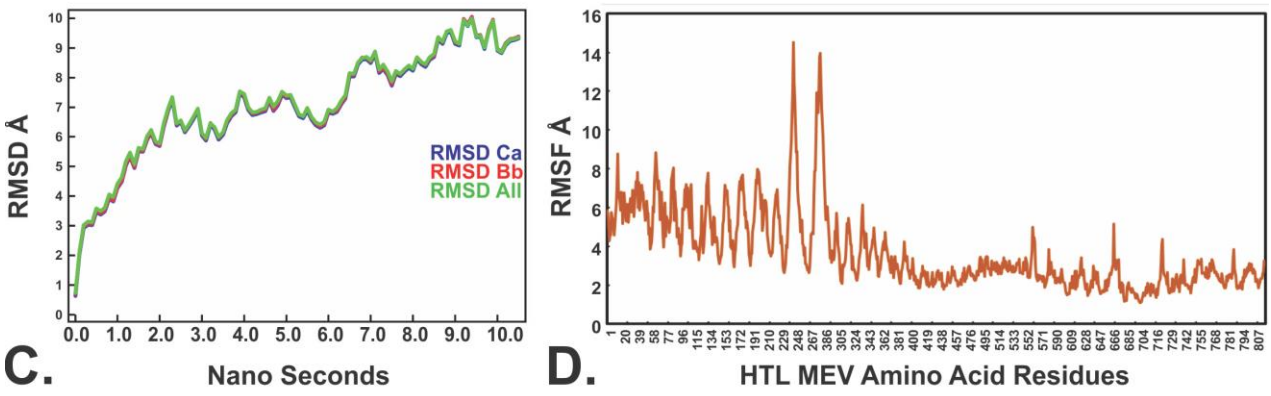

HTL Multi-epitope COVID19 vaccine - Toll Like Receptor 3 complex

Figure 10. Molecular Dynamics simulation of CTL and HTL MEVs with TLR-3 receptor. (A), (C): Root Mean Square Deviation (RMSD) for Cα, Back bone and all atoms (RMSD Ca, RMSD Bb, & RMSD All) respectivally for The CTL MEV – TLR3 complex and The HTL MEV – TLR3 complex. , docking complex of CTL-TLR and HTL-TLR3 have been shown. **(B), (D):** Root Mean Square Fluctuation (RMSF) for all the amino acid residues of CTL MEV and the HTL MEV in complex with TLR3 immune receptor.

***In-silico* analysis of MEVs for cloning and expression potency**

Analysis of cDNA of both the MEVs for cloning and expression in the mammalian host cell line. Complementary DNA optimized for CTL and HTL expression in the mammalian host cell line (Human) was generated by utilizing the Java Codon Adaptation Tool. Further, the generated optimized cDNA's for both the MEVs were analyzed by utilizing the GenScript Rare Codon Analysis Tool. The analysis revealed that the codon-optimized cDNA of both the CTL and HTL MEVs bear all the crucial and favorable compositions for high- level expression in a mammalian cell line (CTL-MEV: GC content 70.40%, CAI (Codon Adaptation Index) score 1.00 and 0% tandem rare codons; HTL MEV: GC content 69.26%, CAI score 1.00 and 0% tandem rare codons). Ideally, the GC content of a cDNA should be 30% to 70%, CAI score that indicates the possibility of cDNA expression in a chosen expression system should be between 0.8-1.0, and the tandem rare codon frequency that indicates the presence of low-frequency codons in cDNA should be <30%. The tandem rare codons may hinder the proper expression of

the cDNA or even interrupt the translational machinery of the chosen expression system. Hence as per the GenScript Rare Codon analysis, the cDNA of both the MEVs satisfies all the mentioned parameters and are predicted to have high expression in the mammalian host cell line (Human).

CONCLUSION

In the present study, we have designed and proposed two multi-epitope vaccines derived from multiple CTL and HTL epitopes against SARS-CoV-2 (COVID19). The chosen CTL and HTL epitopes show significant sequence overlap with screened linear B cell epitopes. The shortlisted CTL and HTL epitopes were utilized to design CTL and HTL multi-epitope vaccine. Both the generated CTL and HTL multi-epitope vaccine tertiary models have shown to carry potential linear and discontinuous B cell epitopes as well as potential INF-γ epitopes. Hence the designed MEVs are predicted to have the potential to elicit humoral as well as cellular immune responses. Since Onchocerca volvulus activation-associated secreted protein-1 (Ov-ASP-1) binds to the APCs and trigger pro-inflammatory cytokine production via Toll-like receptor 3 (TLR3), the truncated (residues 10-153) Ov-ASP-1 has been utilized as an adjuvant at N terminal of both the CTL and HTL MEVs models. Chosen overlapping clustering epitopes were validated for their molecular interaction with their respective HLA allele binders by molecular docking studies. The molecular interaction of the chosen CTL epitopes within the TAP transporter cavity was also analyzed. Analysis of the average world population coverage by both the shortlisted CTL

and HTL epitopes combined revealed coverage of 96.10% world population. The molecular interaction analysis of both the CTL and HTL MEVs with the immunoreceptor TLR3 has shown very convincing structural fitting of the MEVs into the ectodomain of TLR3 receptor cavity. This result was further confirmed by the molecular dynamics simulation studies of both the CTL MEV – TLR3 and HTL MEV – TLR3 complexes, indicating stable molecular complex formation tendency for both the MEVs in complex with TLR3. The cDNA for both the MEVs was generated considering codon-biasing for expression in the mammalian host cell line (Human). Both the cDNA has been optimized in respect of their GC content and zero tandem rare codons for the cDNA to have high expression possibility in the mammalian host cell line (Human). Hence for further studies, both the design of CTL and HTL MEVs could be cloned, expressed and tested for *in-vivo* validations and animal trials as potential vaccine candidates against SARS-CoV-2 infection.

Supplementary table S1. Homology modeling for HLA alleles. Tertiary structures of HLA alleles were modeled by homology modeling using SwissModel server. Templates were chosen with the highest sequence identity. Generated models with acceptable QMEAN values were chosen for further studies.

Supplementary table S2. INF-γ epitopes from CTL and HTL MEVs. INF-γ inducing (POSITIVE) epitopes from CTL and HTL MEVs were screened by using "Motif and SVM hybrid" (MERCI & SVM) approach.

Supplementary table S3. Refinement models of CTL and HTL MEVs. Both the CTL and HTL MEVs models were refined by GalaxyWEB server. After refinement, in particular the Rama favored residues increased significantly.

Supplementary table S4. B Cell linear epitopes of CTL MEVs. Linear B Cell epitopes predicted by ElliPro (IEDB) from CTL MEVs.

Supplementary table S5. B Cell discontinuous epitopes of CTL MEVs. Discontinuous B Cell epitopes predicted by ElliPro (IEDB) from CTL MEVs.

Supplementary table S6. B Cell linear epitopes of HTL MEVs. Linear B Cell epitopes predicted by ElliPro (IEDB) from HTL MEVs.

Supplementary table S7. B Cell discontinuous epitopes of HTL MEVs. Discontinuous B Cell epitopes predicted by ElliPro (IEDB) from HTL MEVs.

Supplementary table S8. Shortlisted high scoring CTL epitopes (MHC-I Binding Predictions). Selected high scoring CTL epitopes and their respective HLA alleles binders predicted by "MHC-I Binding Predictions" IEDB tool. *In-silico* analysis has shown all the selected epitopes to be non-toxic (Non-Toxin) as well as they show significant conservancy and high immunogenicity.

Supplementary table S9. Shortlisted high scoring CTL epitopes (MHC-I Processing Predictions). Selected high scoring CTL epitopes and their respective HLA alleles binders predicted by "MHC-I Processing Predictions" IEDB tool. The screening gives detailed and combined scoring "Total score" for Proteasomal cleavage/TAP transport/MHC class I combined. *In-silico* analysis have shown all the selected epitopes to be non-toxic (Non-Toxin) as well as they show significant conservancy with high immunogenicity.

Supplementary table S10. Shortlisted high scoring HTL epitopes (MHC-II Binding Predictions). Selected high "Percentile rank" HTL epitopes with their respective HLA class II alleles binders predicted by the "**MHC-II Binding Predictions**" tool of IEDB are listed. *In-silico* analysis has shown all the selected epitopes to be non-toxic (Non-Toxin) as well as they show significant conservancy.

Supplementary table S11. Shortlisted B Cell epitopes (BepiPred Linear B Cell Prediction). B cell linear epitopes with length of 4 to 20 amino acids, predicted by the "BepiPred Linear B Cell Prediction" IEDB tool, from eleven SARS-CoV-2 proteins, are listed here. *In-silico* analysis has shown all the selected epitopes to be non-toxic (Non-Toxin) as well as they show significant amino acid sequence conservancy.

AUTHOR CONTRIBUTION:

Protocol design: S.S., M.K.; Methodology performed by S.S., S.V., M.K., R.K.;

Global Economic risk analysis: R.K.B.; Data analysis, scientific writing and

revising the article: S.S., S.V., M.K., R.K., R.K.B., A.K.S., H.J.S., M.Kolbe, KCP.

ADDITIONAL INFORMATION:

Authors declare to have no competing interests.

REFERENCES:

Abele, R. and Tampé, R., 2004. The ABCs of immunology: structure and function of TAP, the transporter associated with antigen processing. Physiology, 19(4), pp.216-224.

Antoniou, A.N., Powis, S.J. and Elliott, T., 2003. Assembly and export of MHC class I peptide ligands. Current opinion in immunology, 15(1), pp.75-81.

Arnold K, Bordoli L, Kopp J, and Schwede T (2006). The SWISS-MODEL Workspace: A web-based environment for protein structure homology modelling. Bioinformatics.,22,195-201.

Bell, J.K., Botos, I., Hall, P.R., Askins, J., Shiloach, J., Segal, D.M. and Davies, D.R., 2005. The molecular structure of the Toll-like receptor 3 ligand-binding domain. Proceedings of the National Academy of Sciences of the United States of America, 102(31), pp.10976-10980.

Benkert, P., Tosatto, S.C. and Schomburg, D., 2008. QMEAN: A comprehensive scoring function for model quality assessment. Proteins: Structure, Function, and Bioinformatics, 71(1), pp.261-277.

Bui H. H, Sidney J, Dinh K, Southwood S, Newman M. J, Sette A. 2006. Predicting population coverage of T-cell epitope-based diagnostics and vaccines. BMC Bioinformatics 17:153.

Bui HH, Sidney J, Li W, Fusseder N, Sette A. 2007. Development of an epitope conservancy analysis tool to facilitate the design of epitope-based diagnostics and vaccines. BMC Bioinformatics 8:361.

Calis JJA, Maybeno M, Greenbaum JA, Weiskopf D, De Silva AD, Sette A, Kesmir C, Peters B. 2013. Properties of MHC class I presented peptides that enhance immunogenicity. PloS Comp. Biol. 8(1):361.

Case, D.A., Babin, V., Berryman, J.T., Betz, R.M., Cai, Q., Cerutti, D.S., Cheatham III, T.E., Darden, T.A., Duke, R.E., Gohlke, H. and Goetz, A.W., 2014. The FF14SB force field. Amber, 14, pp.29-31.

Chen, X., Zaro, J.L. and Shen, W.C., 2013. Fusion protein linkers: property,

1307 design and functionality. Advanced drug delivery reviews, 65(10),
1308 pp.1357-1369.
1309 Delneste, Y., Beauvillain, C. and Jeannin, P., 2007. Innate immunity: structure
1310 and function of TLRs. Medecine sciences: M/S, 23(1), pp.67-73.
1311 Dhanda, S. K., Vir, P. & Raghava, G. P. Designing of interferon-gamma inducing
1312 MHC class-II binders. Biol. Direct. 8, 30 (2013).
1313 Dong Xu and Yang Zhang. Improving the Physical Realism and Structural
1314 Accuracy of Protein Models by a Two-step Atomic-level Energy
1315 Minimization. Biophysical Journal, vol 101, 2525-2534 (2011).
1316 Duhovny D, Nussinov R, Wolfson HJ. Efficient Unbound Docking of Rigid
1317 Molecules. In Gusfield et al., Ed. Proceedings of the 2'nd Workshop on
1318 Algorithms in Bioinformatics(WABI) Rome, Italy, Lecture Notes in
1319 Computer Science 2452, pp. 185-200, Springer Verlag, 2002
1320 Farina, C., Krumbholz, M., Giese, T., Hartmann, G., Aloisi, F. and Meinl, E.,
1321 2005. Preferential expression and function of Toll-like receptor 3 in human
1322 astrocytes. Journal of neuroimmunology, 159(1-2), pp.12-19.
1323 Gasteiger, E., Hoogland, C., Gattiker, A., Duvaud, S.E., Wilkins, M.R., Appel,
1324 R.D. and Bairoch, A., 2005. Protein identification and analysis tools on the
1325 ExPASy server (pp. 571-607). Humana Press.
1326 Grifoni, A., Sidney, J., Zhang, Y., Scheuermann, R.H., Peters, B. and Sette, A.,
1327 2020. A Sequence Homology and Bioinformatic Approach Can Predict
1328 Candidate Targets for Immune Responses to SARS-CoV-2. Cell Host &
1329 Microbe.
1330 Guo, J., Yang, Y., Xiao, W., Sun, W., Yu, H., Du, L., Lustigman, S., Jiang, S.,
1331 Kou, Z. and Zhou, Y., 2015. A truncated fragment of Ov-ASP-1 consisting
1332 of the core pathogenesis-related-1 (PR-1) domain maintains adjuvanticity
1333 as the full-length protein. Vaccine, 33(16), pp.1974-1980.
1334 Gupta, S., Kapoor, P., Chaudhary, K., Gautam, A., Kumar, R., Raghava, G.P.
1335 and Open Source Drug Discovery Consortium, 2013. In silico approach for
1336 predicting toxicity of peptides and proteins. PLoS One, 8(9), p.e73957.
1337 Hajighahramani, N., Nezafat, N., Eslami, M., Negahdaripour, M., Rahmatabadi,
1338 S.S. and Ghasemi, Y., 2017. Immunoinformatics analysis and in silico
1339 designing of a novel multi-epitope peptide vaccine against Staphylococcus
1340 aureus. Infection, Genetics and Evolution, 48, pp.83-94.
1341 He, Y., Barker, S.J., MacDonald, A.J., Yu, Y., Cao, L., Li, J., Parhar, R., Heck, S.,
1342 Hartmann, S., Golenbock, D.T. and Jiang, S., 2009. Recombinant Ov-
1343 ASP-1, a Th1-biased protein adjuvant derived from the helminth
1344 Onchocerca volvulus, can directly bind and activate antigen-presenting
1345 cells. The Journal of Immunology, 182(7), pp.4005-4016.
1346 Hoof, I., Peters, B., Sidney, J., Pedersen, L.E., Sette, A., Lund, O., Buus, S. and

1347 Nielsen, M., 2009. NetMHCpan, a method for MHC class I binding
1348 prediction beyond humans. Immunogenetics, 61(1), p.1.
1349 Hu W, Li F, Yang X, Li Z, Xia H, Li G, Wang Y, Zhang Z. A flexible peptide linker
1350 enhances the immunoreactivity of two copies HBsAg preS1 (21-47) fusion
1351 protein. J Biotechnol. 2004;107:83–90.
1352 Irini A Doytchinova and Darren R Flower. VaxiJen: a server for prediction of
1353 protective antigens, tumour antigens and subunit vaccines. BMC
1354 Bioinformatics. 2007 8:4.
1355 Ko, J., Park, H., Heo, L., and Seok, C., GalaxyWEB server for protein structure
1356 prediction and refinement, Nucleic Acids Res. 40 (W1), W294-W297
1357 (2012).
1358 Krieger, E. and Vriend, G., 2015. New ways to boost molecular dynamics
1359 simulations. Journal of computational chemistry, 36(13), pp.996-1007.
1360 Kringelum, J.V., Lundegaard, C., Lund, O. and Nielsen, M., 2012. Reliable B cell
1361 epitope predictions: impacts of method development and improved
1362 benchmarking. PLoS computational biology, 8(12).
1363 Larsen JE, Lund O, Nielsen M. 2006. Improved method for predicting linear B-
1364 cell epitopes. Immunome Res 2:2.
1365 MacDonald, A.J., Cao, L., He, Y., Zhao, Q., Jiang, S. and Lustigman, S., 2005.
1366 rOv-ASP-1, a recombinant secreted protein of the helminth Onchocerca
1367 volvulus, is a potent adjuvant for inducing antibodies to ovalbumin, HIV-1
1368 polypeptide and SARS-CoV peptide antigens. Vaccine, 23(26), pp.3446-
1369 3452.
1370 Maier, J.A., Martinez, C., Kasavajhala, K., Wickstrom, L., Hauser, K.E. and
1371 Simmerling, C., 2015. ff14SB: improving the accuracy of protein side chain
1372 and backbone parameters from ff99SB. Journal of chemical theory and
1373 computation, 11(8), pp.3696-3713.
1374 Morla, S., Makhija, A. & Kumar, S. Synonymous codon usage pattern in
1375 glycoprotein gene of rabies virus. Gene. 584, 1–6 (2016).
1376 Nagpal, G., Gupta, S., Chaudhary, K., Dhanda, S.K., Prakash, S. and Raghava,
1377 G.P., 2015. VaccineDA: Prediction, design and genome-wide screening of
1378 oligodeoxynucleotide-based vaccine adjuvants. Scientific reports, 5,
1379 p.12478.
1380 NCBI protein sequence database: SARS-CoV-2 (Severe acute respiratory
1381 syndrome coronavirus 2) Sequences
1382 (https://www.ncbi.nlm.nih.gov/genbank/sars-cov-2-seqs/)
1383 Nielsen, M., Lundegaard, C. and Lund, O., 2007. Prediction of MHC class II
1384 binding affinity using SMM-align, a novel stabilization matrix alignment
1385 method. BMC bioinformatics, 8(1), p.238.
1386 Oldham, M.L., Grigorieff, N. and Chen, J., 2016. Structure of the Transporter

associated with antigen processing trapped by herpes simplex virus. eLife, 5, p.e21829.

Peters B, Bulik S, Tampe R, Van Endert PM, Holzhutter HG. 2003. Identifying MHC class I epitopes by predicting the TAP transport efficiency of epitope precursors. J Immunol171:1741-1749.

Pettersen, E.F., Goddard, T.D., Huang, C.C., Couch, G.S., Greenblatt, D.M., Meng, E.C. and Ferrin, T.E., 2004. UCSF Chimera—a visualization system for exploratory research and analysis. Journal of computational chemistry, 25(13), pp.1605-1612.

Ponomarenko JV, Bui H, Li W, Fusseder N, Bourne PE, Sette A, Peters B. 2008. ElliPro: a new structure-based tool for the prediction of antibody epitopes. BMC Bioinformatics 9:514.

PyMOL: The PyMOL Molecular Graphics System, Version 2.0 Schrödinger, LLC.

Ramakrishnan, C. and Ramachandran, G.N., 1965. Stereochemical criteria for polypeptide and protein chain conformations: II. Allowed conformations for a pair of peptide units. Biophysical journal, 5(6), pp.909-933.

Roy, A., Kucukural, A. and Zhang, Y., 2010. I-TASSER: a unified platform for automated protein structure and function prediction. Nature protocols, 5(4), p.725.

S.C. Lovell, I.W. Davis, W.B. Arendall III, P.I.W. de Bakker, J.M. Word, M.G. Prisant, J.S. Richardson and D.C. Richardson (2002) Structure validation by Calpha geometry: phi,psi and Cbeta deviation. Proteins: Structure, Function & Genetics. 50: 437-450.

Saha, S. & Raghava, G. AlgPred: prediction of allergenic proteins and mapping of IgE epitopes. Nucleic. Acids. Res. 34, W202–W209 (2006).

Schneidman-Duhovny D, Inbar Y, Nussinov R, Wolfson HJ. PatchDock and SymmDock: servers for rigid and symmetric docking. Nucl. Acids. Res. 33: W363-367, 2005.

Shen, Y., Maupetit, J., Derreumaux, P. and Tufféry, P., 2014. Improved PEP-FOLD approach for peptide and miniprotein structure prediction. Journal of chemical theory and computation, 10(10), pp.4745-4758.

Shin, W.H., Lee, G.R., Heo, L., Lee, H. and Seok, C., 2014. Prediction of protein structure and interaction by GALAXY protein modeling programs. Bio Design, 2(1), pp.1-11.

Sidney, J., Assarsson, E., Moore, C., Ngo, S., Pinilla, C., Sette, A. and Peters, B., 2008. Quantitative peptide binding motifs for 19 human and mouse MHC class I molecules derived using positional scanning combinatorial peptide libraries. Immunome research, 4(1), p.2.

Sievers, F., Wilm, A., Dineen, D., Gibson, T.J., Karplus, K., Li, W., Lopez, R., McWilliam, H., Remmert, M., Söding, J. and Thompson, J.D., and Higgins

1427 D.G., 2011. Fast, scalable generation of high-quality protein multiple
1428 sequence alignments using Clustal Omega. Molecular systems biology,
1429 7(1), p.539.
1430 Srivastava, S., Kamthania, M., Kumar Pandey, R., Kumar Saxena, A., Saxena,
1431 V., Kumar Singh, S., Kumar Sharma, R. and Sharma, N., 2019. Design of
1432 novel multi-epitope vaccines against severe acute respiratory syndrome
1433 validated through multistage molecular interaction and dynamics. Journal
1434 of Biomolecular Structure and Dynamics, 37(16), pp.4345-4360.
1435 Srivastava, S., Kamthania, M., Singh, S., Saxena, A.K. and Sharma, N., 2018.
1436 Structural basis of development of multi-epitope vaccine against middle
1437 east respiratory syndrome using in silico approach. Infection and drug
1438 resistance, 11, p.2377.
1439 Sturniolo, T., Bono, E., Ding, J., Raddrizzani, L., Tuereci, O., Sahin, U.,
1440 Braxenthaler, M., Gallazzi, F., Protti, M.P., Sinigaglia, F. and Hammer, J.,
1441 1999. Generation of tissue-specific and promiscuous HLA ligand
1442 databases using DNA microarrays and virtual HLA class II matrices.
1443 Nature biotechnology, 17(6), p.555.
1444 Tenzer S, Peters B, Bulik S, Schoor O, Lemmel C, Schatz MM, Kloetzel PM,
1445 Rammensee HG, Schild H, Holzhutter HG. 2005. Modeling the MHC class
1446 I pathway by combining predictions of proteasomal cleavage, TAP
1447 transport and MHC class I binding. Cell Mol Life Sci 62:1025-1037.
1448 Totura, A.L., Whitmore, A., Agnihothram, S., Schäfer, A., Katze, M.G., Heise,
1449 M.T. and Baric, R.S., 2015. Toll-like receptor 3 signaling via TRIF
1450 contributes to a protective innate immune response to severe acute
1451 respiratory syndrome coronavirus infection. MBio, 6(3), pp.e00638-15.
1452 Toukmaji, A., Sagui, C., Board, J. and Darden, T., 2000. Efficient particle-mesh
1453 Ewald based approach to fixed and induced dipolar interactions. The
1454 Journal of chemical physics, 113(24), pp.10913-10927.
1455 United nations conference on trade and development report 9th March 2020
1456 (https://unctad.org/en/pages/PressRelease.aspx?OriginalVersionID=548)
1457 Wang, P., Sidney, J., Kim, Y., Sette, A., Lund, O., Nielsen, M. and Peters, B.,
1458 2010. Peptide binding predictions for HLA DR, DP and DQ molecules.
1459 BMC bioinformatics, 11(1), p.568.
1460 Wang, Z. and Xu, J., 2013. Predicting protein contact map using evolutionary and
1461 physical constraints by integer programming. Bioinformatics, 29(13),
1462 pp.i266-i273.
1463 World Health Organization report, Coronavirus disease 2019 (COVID-19)
1464 Situation Report – 61, 21st March 2020 (https://www.who.int/docs/default-
1465 source/coronaviruse/situation-reports/20200321-sitrep-61-covid-
1466 19.pdf?sfvrsn=6aa18912_2)

Wu, X., Wu, S., Li, D., Zhang, J., Hou, L., Ma, J., Liu, W., Ren, D., Zhu, Y. and He, F., 2010. Computational identification of rare codons of Escherichia coli based on codon pairs preference. Bmc Bioinformatics, 11(1), p.61.

Eleven SARS-CoV-2 proteins were chosen
Protein sequences retrieved from NCBI

Screening of potential CTL, HTL and B Cell epitopes

Screening of CTL epitope *(IEDB "MHC-I Binding Predictions" and "MHC-I Processing Predictions")*

Screening of HTL epitopes *(IEDB "MHC-II Binding Predictions")*

Screening of protein sequence based B Cell epitope *(IEDB "B Cell Epitope Prediction Tools")*

Population coverage by screened CTL and HTL epitopes *(IEDB "Population Coverage")*

Characterization of screened potential epitopes

Epitope conservation analysis *(IEDB "Epitope Conservancy Analysis")*

Epitope toxicity prediction *(ToxinPred)*

Overlapping residue analysis for CTL, HTL & B Cell epitopes *(Clustal Omega)*

Molecular interaction study of selected overlapping CTL & HTL epitopes with HLA allele and TAP transporter

3D structure modelling of HLA alleles and selected CTL & HTL epitopes *(Swiss-model & PEP-FOLD2.0)*

Molecular interaction analysis of selected overlapping Ctl and HTL epitopes with HLA allele *(PatchDock Tool)*

Molecular interaction analysis of selected CTL epitopes with TAP transporter *(PatchDock Tool)*

Design and characterisation of CTL & HTL Multi-Epitope Vaccines

Interferon gama inducing epitope prediction from designed MEVs *("IFNepitope")*

MEVs allergenicity and antigenicity prediction *(AlgPred & VaxiJen)*

Physicochemical analysis of MEVs *(ProtParam)*

3D structure modelling and refinement of CTL & HTL MEVs *(I-TASSER, ModRefiner, GalaxyWEB)*

***In-silico* validation of refined CTL & HTL MEV models** *(RAMPAGE)*

Discontinuous B-cell epitope prediction from CTL & HTL MEVs *(IEDB "ElliPro")*

Molecular interaction analysis of CTL & HTL MEVs with TLR3
(PatchDock)

***In-silico* analysis of cDNA of CTL & HTL MEVs for cloning and expression in mammalian cell line (Human)**
(Codon Usage Wrangler Tool & GenScript Rare Codon Analysis Tool)

A. CTL epitopes

B. HTL epitopes

Ov-ASP-1 *(truncated (10-153))*

IVVAVTGYNCPGGKLTALERKKIVGQNNKYRSDLINGKL
KNRNGTYMPRGKNMLELTWDCKLESSAQRWANQCIFG
HSPRQQREGVGENVYAYWSSVSVEGLKKTAGTDAGKS
WWSKLPKLYENNPSNNMTWKVAGQGVLHFTQ

	B. HTL epitopes	A. CTL epitopes
Envelope protein	EAAAK LLFLAFVVFLLVTLA GGGGS VLLFLAFVVFLLVTL GGGGS GLMWLSYFIASFRLF GGGGS LMWLSYFIASFRLFA GGGGS LSYYKLGASQRVAGD GGGGS	EAAAK LLFLAFVVF GGGGS LTALRLCAY GGGGS YFIASFRLFAR GGGGS ATSRTLSYYK GGGGS MEVTPSGTW GGGGS KPRQKRTAT
Membrane protein	GGGGS AQFAPSASAFFGMSR GGGGS IAQFAPSASAFFGMS GGGGS PQIAQFAPSASAFFG GGGGS AIILASFSASTSAFV	GGGGS MGYINVFAF GGGGS GYINVFAFPF HHHHHH SEMVMCGGSLY
N protein	GGGGS ESPFVMMSAPPAQYE GGGGS IILASFSASTSAFVE GGGGS QESPFVMMSAPPAQY GGGGS SPFVMMSAPPAQYEL	GGGGS FYWFFSNYLKR GGGGS ISNSWLMW GGGGS ETISLAGSYK GGGGS QEILGTVSW GGGGS STFNVPMEK GGGGS RMYIFFASFY
ORF1ab	GGGGS FVRIATPGQSLP	GGGGS SLFVAAIFYL
ORF3a	GGGGS LLFVTVYSHLLLVAA GGGGS FKVSIWNLDYIINLI GGGGS KVSIWNLDYIINLII GGGGS TFKVSIWNLDYIINL	GGGGS RYFRLTLGVY GGGGS FLNGSCGSV GGGGS CTDDNALAY GGGGS CTDDNALAYY GGGGS MYKGLPWNVVR
ORF6	GGGGS IILFLALITLATCEL GGGGS ILFLALITLATCELY	GGGGS SIINNTVYTK GGGGS LPVNVAFELW
ORF7a	GGGGS CFLAFLLFLVLIMLI GGGGS LCFLAFLLFLVLIML GGGGS YLCFLAFLLFLVLIM	GGGGS DEWSMATYY GGGGS YILFTRFFYV GGGGS YIFFASFYYV
ORF7b	GGGGS CTQHQPYVVDDPCPI GGGGS HQPYVVDDPCPIHFY GGGGS QPYVVDDPCPIHFYS	GGGGS YLYALVYFL GGGGS IPYNSVTSSI GGGGS RTFKVSIW
ORF8	GGGGS INVFAFPFTIYSLLL GGGGS YINVFAFPFTIYSLL	GGGGS AEILLIIMRTF GGGGS RARSVSPK
ORF10	GGGGS KTQSLLIVNNATNVV GGGGS LLIVNNATNVVIKVC	GGGGS QLRARSVSPK GGGGS FLAFLLFLV
Surface protein	GGGGS QSLLIVNNATNVVIK GGGGS SLLIVNNATNVVIKV GGGGS TQSLLIVNNATNVVI HHHHHH	GGGGS HFYSKWYIR GGGGS WTAGAAAYYV GGGGS FPNITNLCPF GGGGS NYNYLYRLFR GGGGS NYLYRLFR HHHHHH

Overlapping T & B cell epitopes across proteome of SARS-CoV-2

ORF1ab	-IILASFSASTSAFVE AIILASFSASTSAFV- 474-489 AIILASFSASTSAFVE ----SPFVMMSAPPAQYEL QESPFVMMSAPPAQY-- -ESPFVMMSAPPAQYE- 1800-1816 QESPFVMMSAPPAQYEL --------YILFTRFFYV---- WFLAYILFTRFFYVL--- -----LAYILFTRFFYVLGL- ---FLAYILFTRFFYVLG-- -------AYILFTRFFYVLGLA 2327-2344 WFLAYILFTRFFYVLGLA -----YIFFASFYYV RMYIFFASFY-- 2382-2393 RMYIFFASFYYV ----------CTDDNALAY--------- ----------CTDDNALAYY------- GTTQTACTDDNALAYYNTTK 4157-4176 GTTQTACTDDNALAYYNTTK RAMPNMLRIMASLVL---- -------PNMLRIMASLVLARK- ---------NMLRIMASLVLARKH ----MPNMLRIMASLVLAR-- --AMPNMLRIMASLVLA--- 5016-5034 RAMPNMLRIMASLVLARKH
Surface protein	--------LLIVNNATNVVIKVC ------SLLIVNNATNVVIKV- ----QSLLIVNNATNVVIK-- --TQSLLIVNNATNVVI--- KTQSLLIVNNATNVV---- 113-131 KTQSLLIVNNATNVVIKVC ----------WTAGAAAYYV TPGDSSSGWTA------- 250-267 TPGDSSSGWTAGAAAYYV FPNITNLCPF---------- FPNITNLCPFGEVFNATRFASVYAWNRKRISNCVA 329-363 FPNITNLCPFGEVFNATRFASVYAWNRKRISNCVA ----------NYNYLYRLFR---------- ----------NYLYRLFR---------- NLDSKVGGNYNYLYRLFRKSNLKPFERDISTEIYQAGSTPCNGVEGFNCYFPLQSYGFQPTN 440-501 NLDSKVGGNYNYLYRLFRKSNLKPFERDISTEIYQAGSTPCNGVEGFNCYFPLQSYGFQPTN
ORF3a	----------FVRATATIPIQASLP QGEIKDATPSDF---------- 17-42 QGEIKDATPSDFVRATATIPIQASLP IPYNSVTSSI -PYNSVT--- 158-167 IPYNSVTSSI
Envelope protein	-LLFLAFVVF------ -LLFLAFVVFLLVTLA VLLFLAFVVFLLVTL- 17-32 VLLFLAFVVFLLVTLA
Membrane Protein	----------YFIASFRLFAR --LMWLSYFIASFRLFA- GLMWLSYFIASFRLF-- 89-105 GLMWLSYFIASFRLFAR ATSRTLSYYK---------- ----------LSYYKLGASQRVAGD- ----------KLGASQRVAGDS 171-191 ATSRTLSYYKLGASQRVAGDS
ORF6	AEILLIIMRTF---------- ----------RTFKVSIW---------- ----------KVSIWNLDYIINLII ----------FKVSIWNLDYIINLI- ----------TFKVSIWNLDYIINL-- 12-37 AEILLIIMRTFKVSIWNLDYIINLII
ORF7a	-ILFLALITLATCELY------- IILFLALITLATCEL-------- ----------LYHYQECVR 3-25 IILFLALITLATCELYHYQECVR ----------RARSVSPK---------- ----------QLRARSVSPK---------- VKHVYQLRARSVSPKLFIRQEEVQEL 71-96 VKHVYQLRARSVSPKLFIRQEEVQEL
ORF7b	------FLAFLLFLV----- ----CFLAFLLFLVLIMLI --LCFLAFLLFLVLIML- YLCFLAFLLFLVLIM-- 10-26 YLCFLAFLLFLVLIMLI
ORF8	----------HFYSKWYIR-------- ----------QPYVVDDPCPIHFYS---------- ----------HQPYVVDDPCPIHFY---------- -----CTQHQPYVVDDPCPI---------- QSCTQHQPYVVDDPCPIHFYSKW---------- ----------RVGARKSAP 23-56 QSCTQHQPYVVDDPCPIHFYSKWYIRVGARKSAP
Nucleocapsid Protein	----------KPRQKRTAT-- RLNQLESKMSGKGQQQQGQTVTKKSAAEASKKPRQKRTATKA 226-267 RLNQLESKMSGKGQQQQGQTVTKKSAAEASKKPRQKRTATKA -----AQFAPSASAFFGMSR ----IAQFAPSASAFFGMS- PQIAQFAPSASAFFG--- 302-319 PQIAQFAPSASAFFGMSR
ORF10	---GYINVFAFPF------ MGYINVFAF-------- -----YINVFAFPFTIYSLL 1-17 MGYINVFAFPFTIYSLL

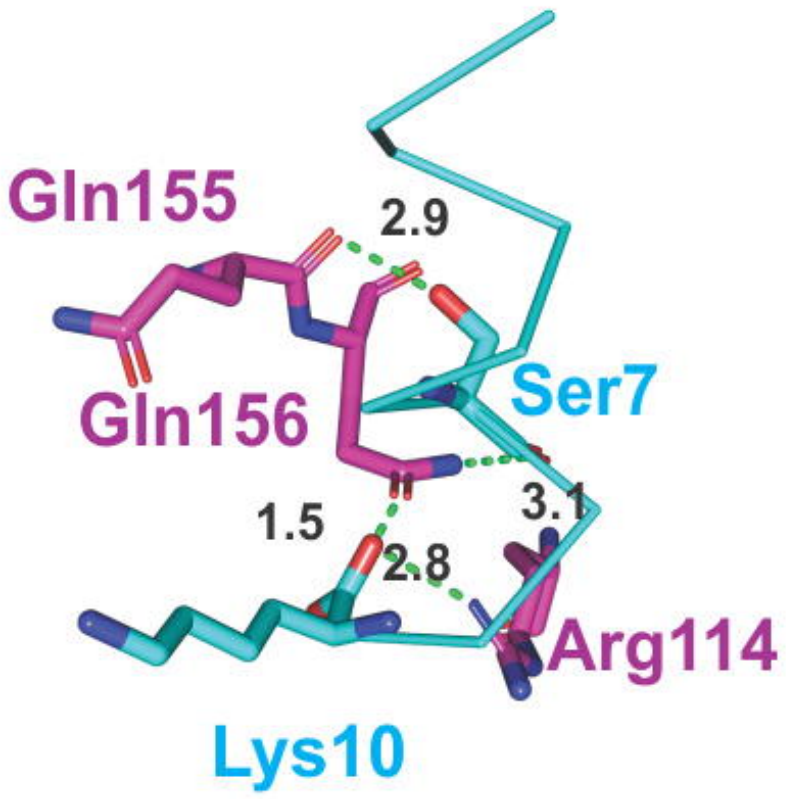

1. ATSRTLSYYK-HLA-A*11:01

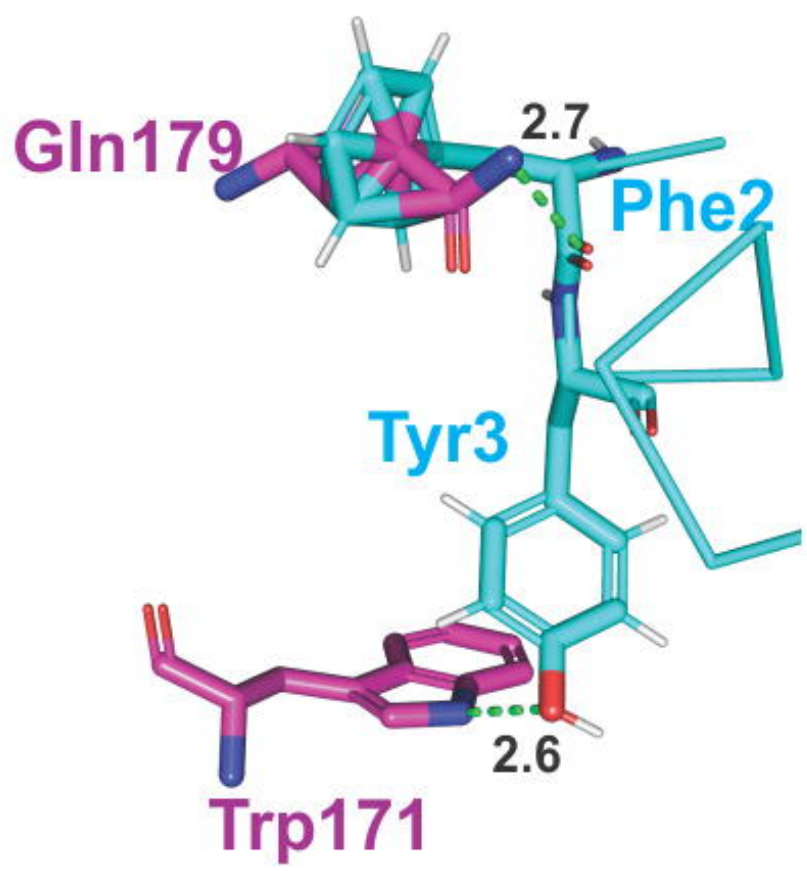

2. HFYSKWYIR-HLA-A*31:01

CTL epitopes - HLA Class I allele complexes

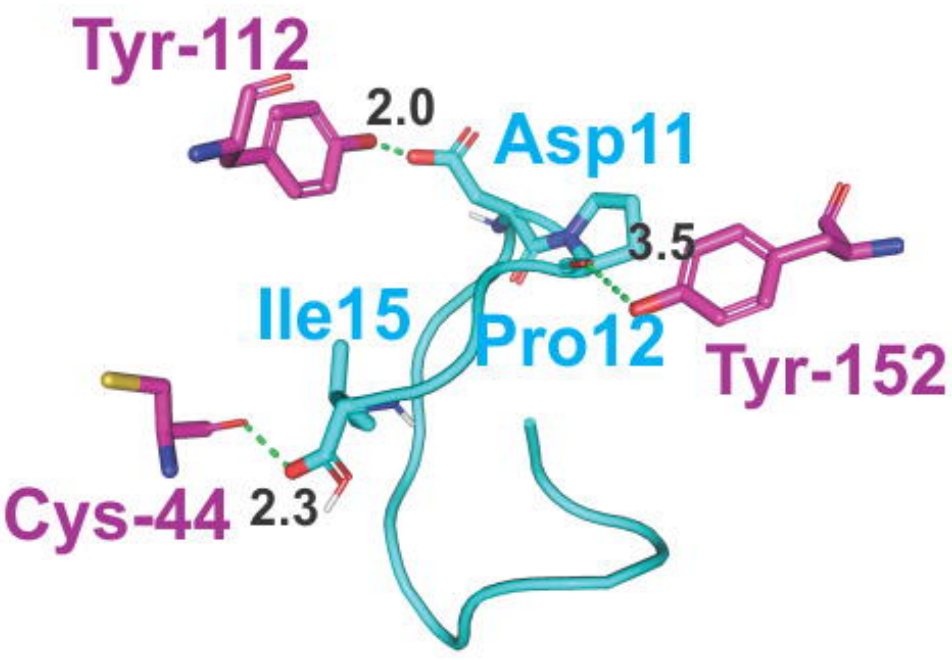

3. CTQHQPYVVDDPCPI-HLA-DRB3*01:01

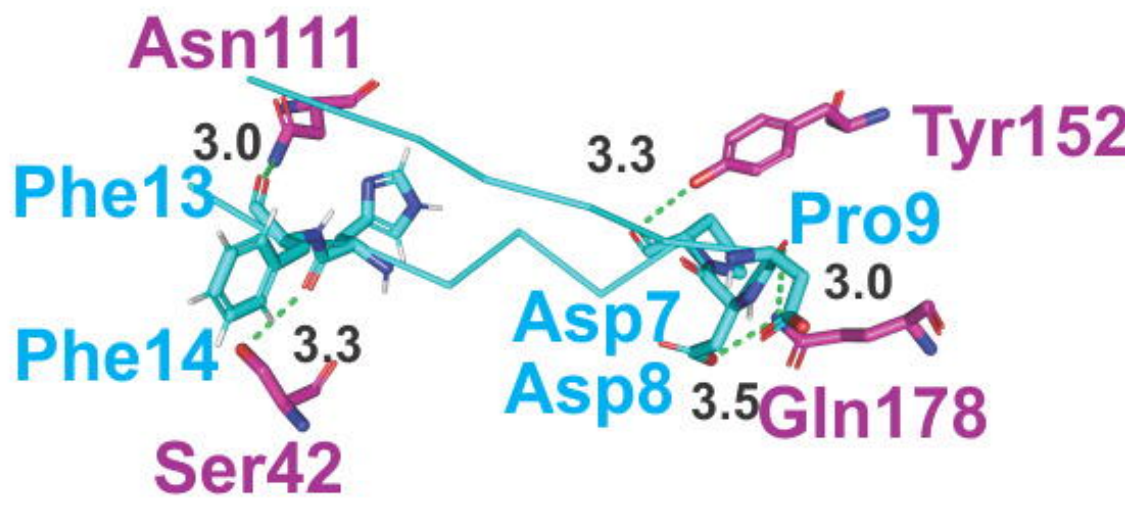

4. HQPYVVDDPCPIHFY-HLA-DRB3*01:01

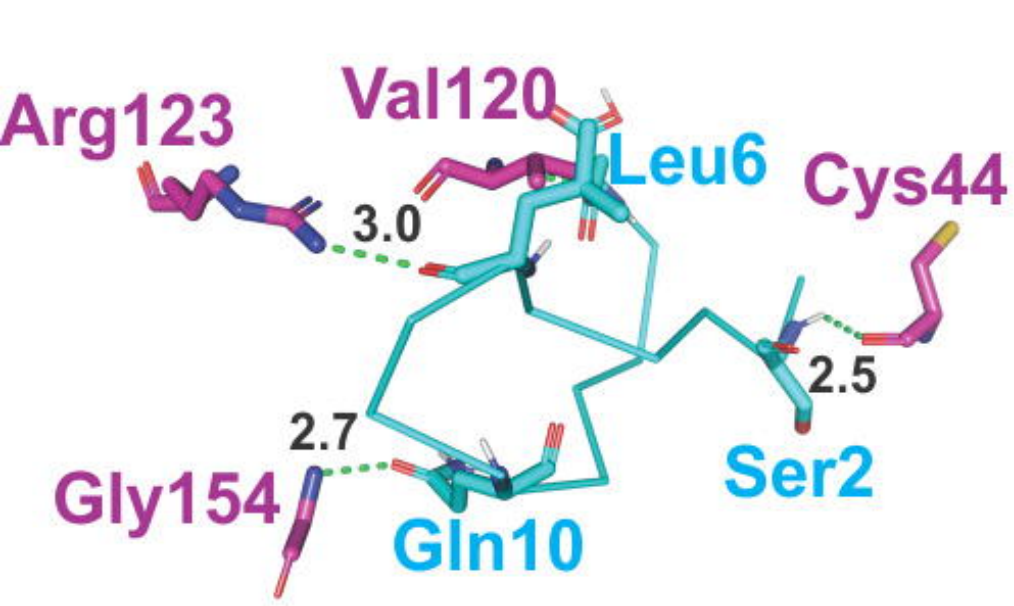

5. LSYYKLGASQRVAGD-HLA-DRB1*09:01

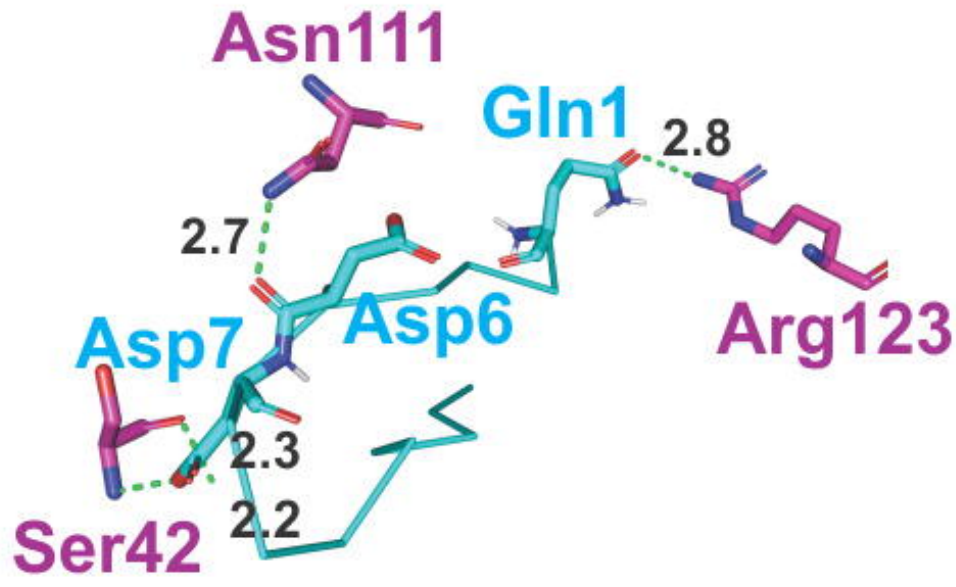

6. QPYVVDDPCPIHFYS-HLA-DRB3*01:01

HTL epitopes - HLA Class II allele complexes

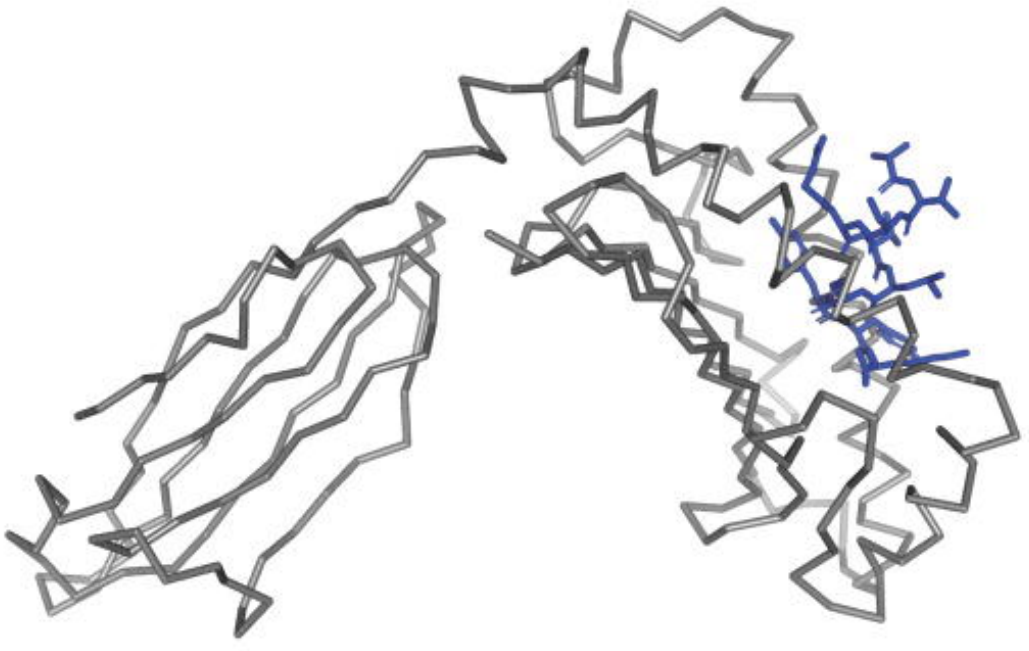

1. ATSRTLSYYK-HLA-A*11:01

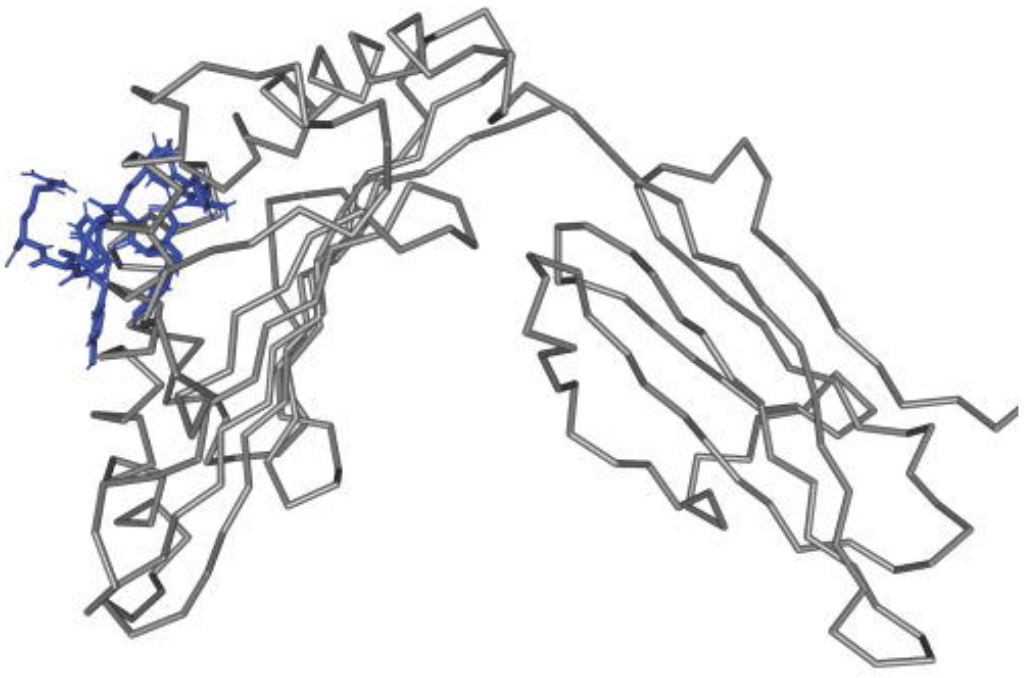

2. HFYSKWYIR-HLA-A*31:01

CTL epitopes - HLA Class I allele complexes

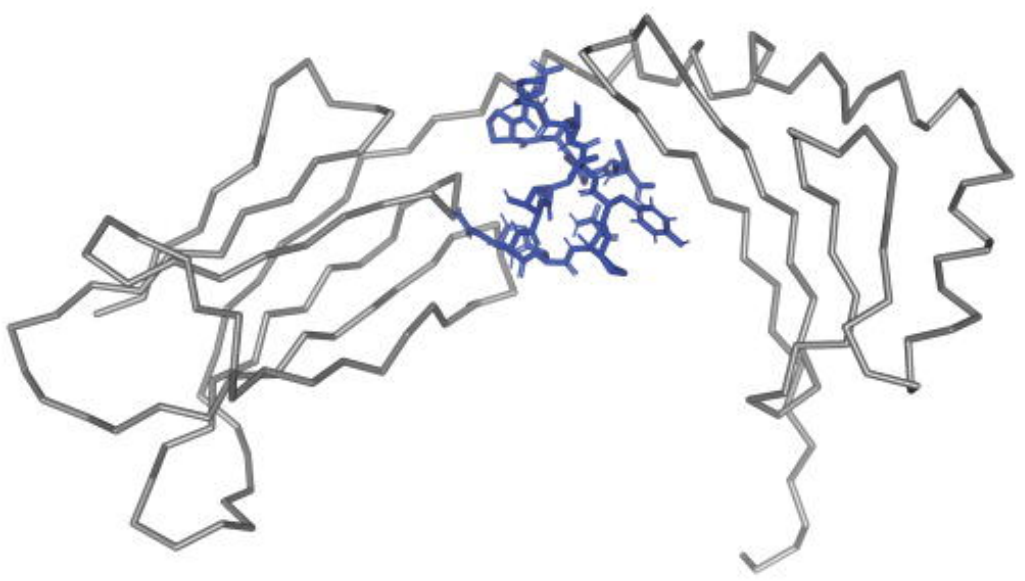

3. CTQHQPYVVDDPCPI-HLA-DRB3*01:01

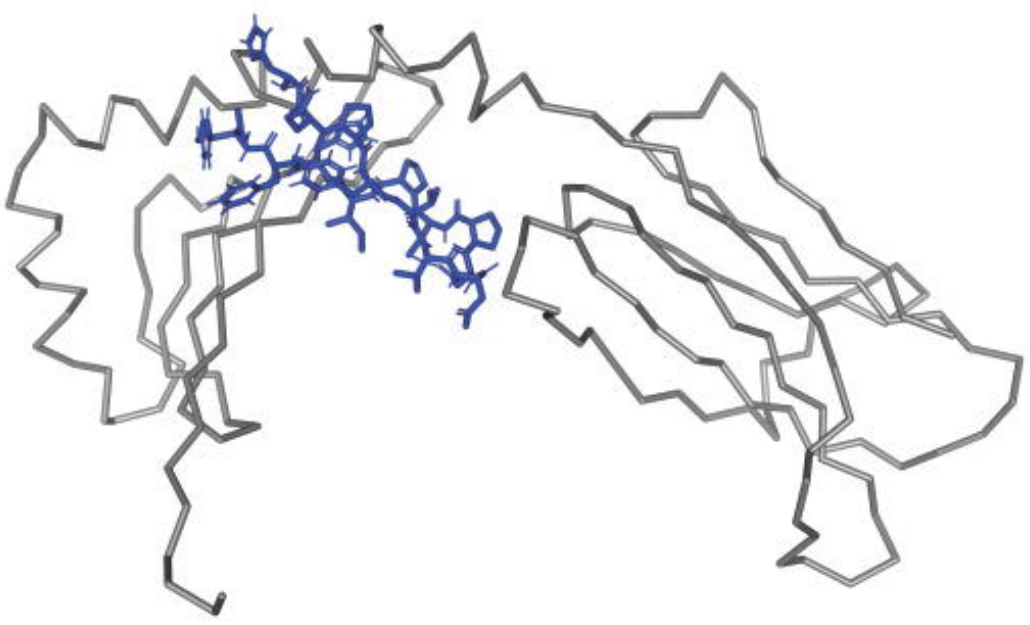

4. HQPYVVDDPCPIHFY-HLA-DRB3*01:01

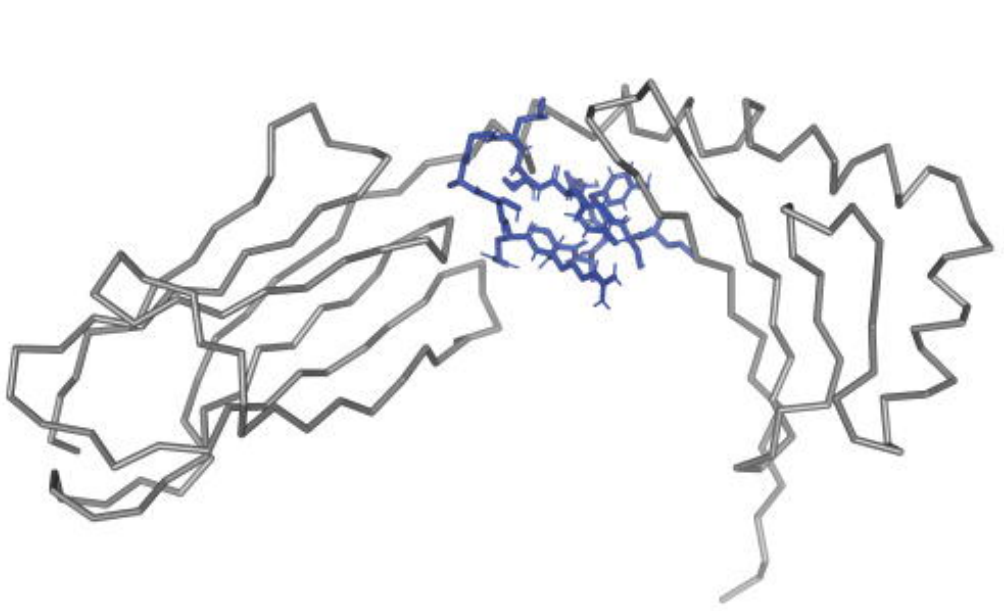

5. LSYYKLGASQRVAGD-HLA-DRB1*09:01

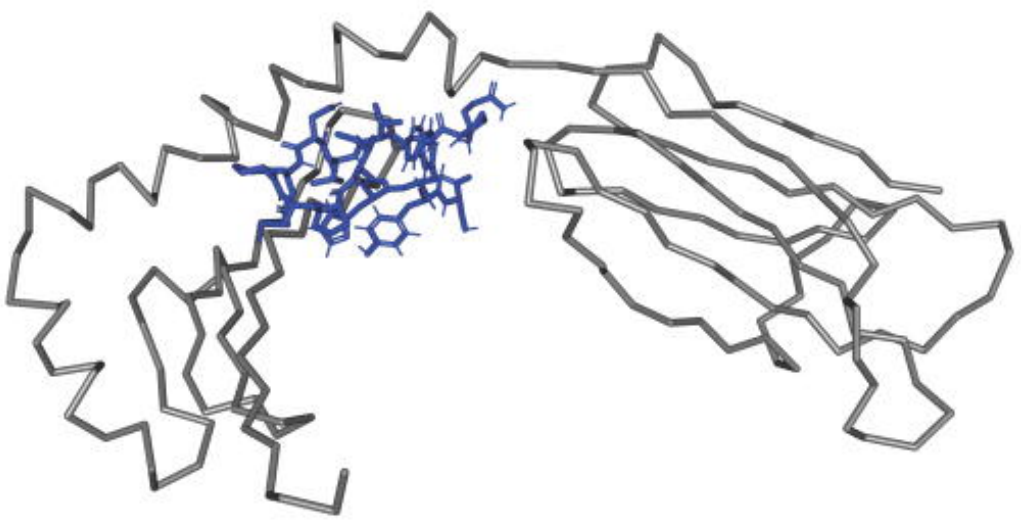

6. QPYVVDDPCPIHFYS-HLA-DRB3*01:01

HTL epitopes - HLA Class II allele complexes

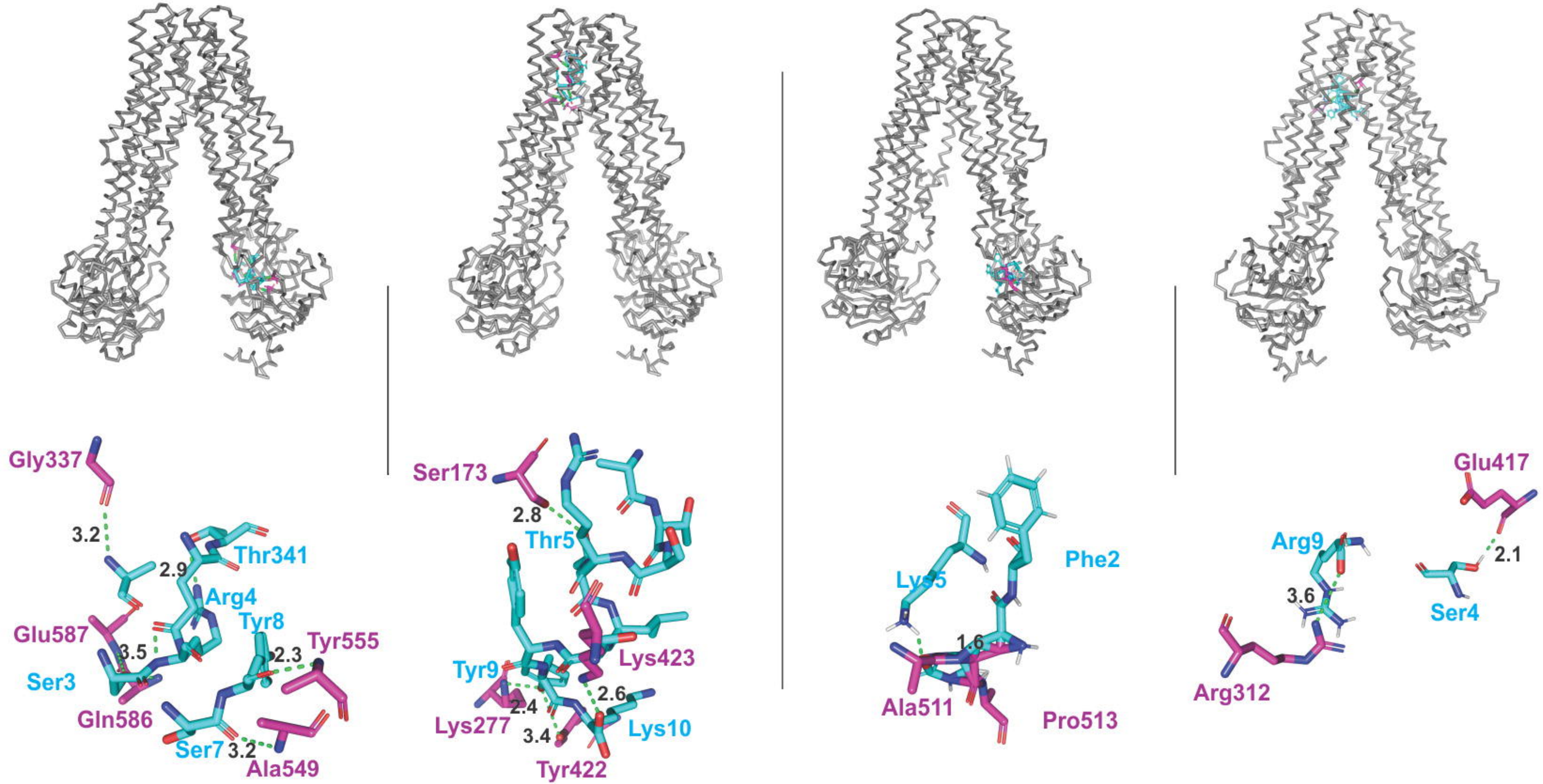

Epitope ATSRTLSYYK through TAP cavity

Epitope HFYSKWYIR through TAP cavity

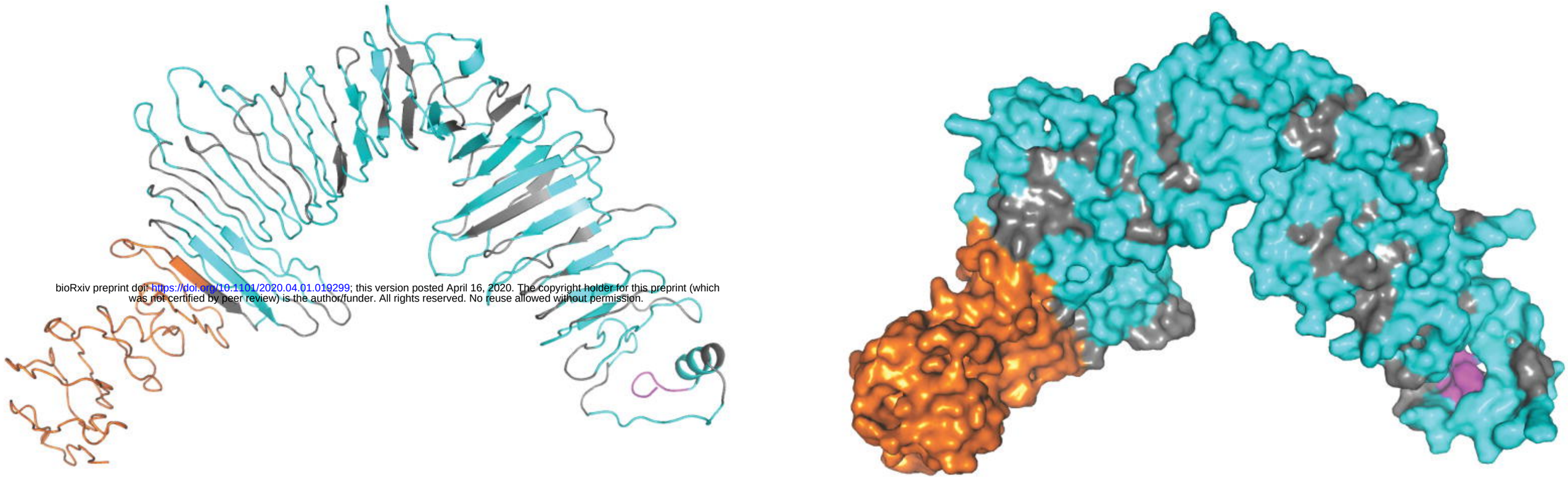

A. CTL Multi-epitope vaccine model

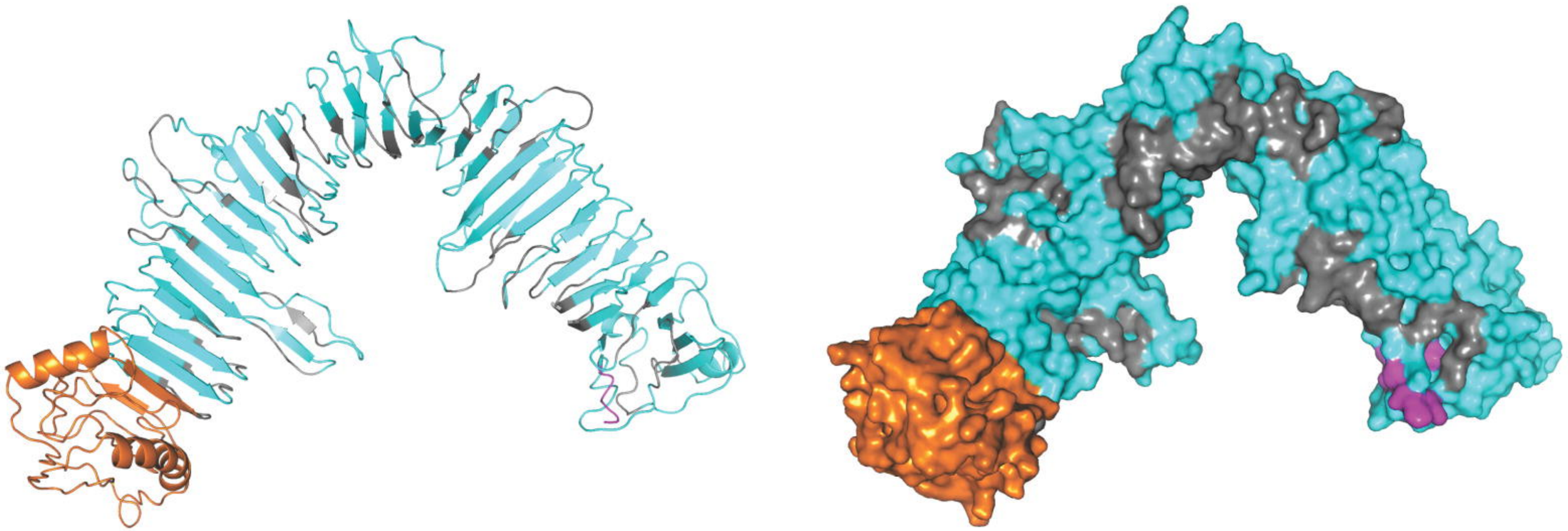

B. HTL Multi-epitope vaccine model

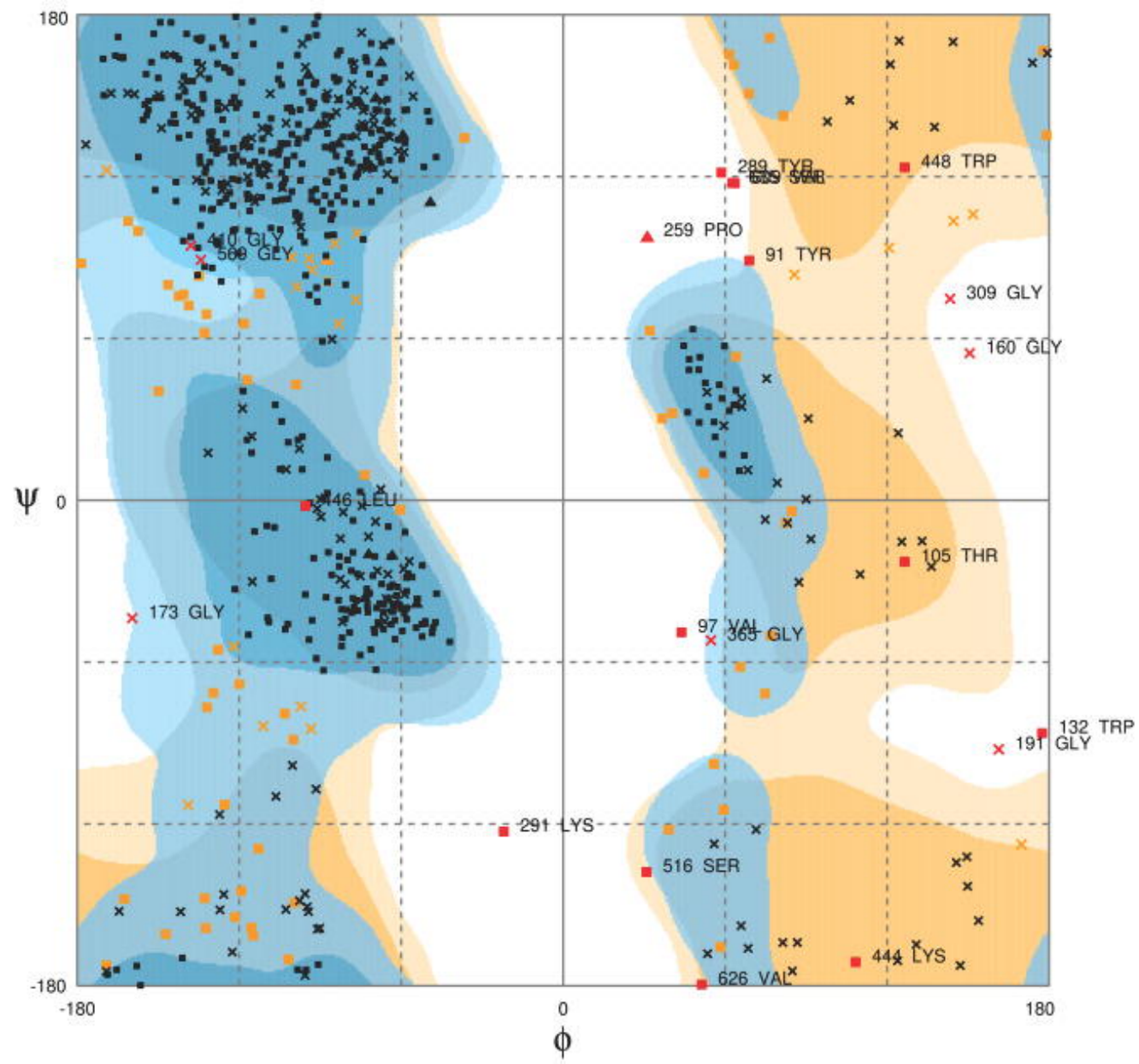

Number of residues in favoured region (~98.0% expected)	: 602 (85.8%)
Number of residues in allowed region (~2.0% expected)	: 79 (11.3%)
Number of residues in outlier region	: 21 (3.0%)

A. CTL Multi-epitope vaccine RAMPAGE analysis

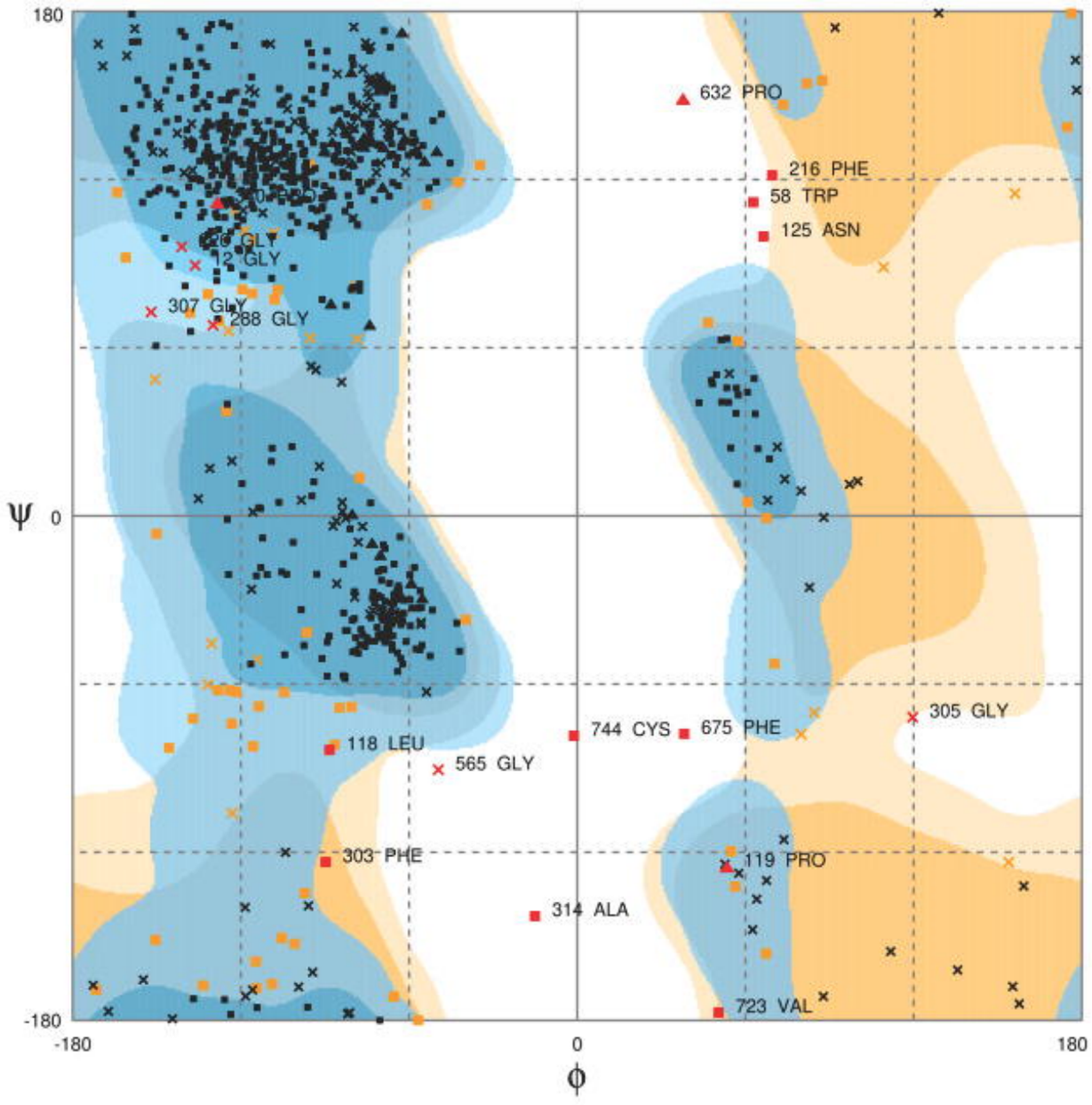

Number of residues in favoured region (~98.0% expected)	: 718 (88.9%)
Number of residues in allowed region (~2.0% expected)	: 72 (8.9%)
Number of residues in outlier region	: 18 (2.2%)

B. HTL Multi-epitope vaccine model RAMPAGE analysis

A.

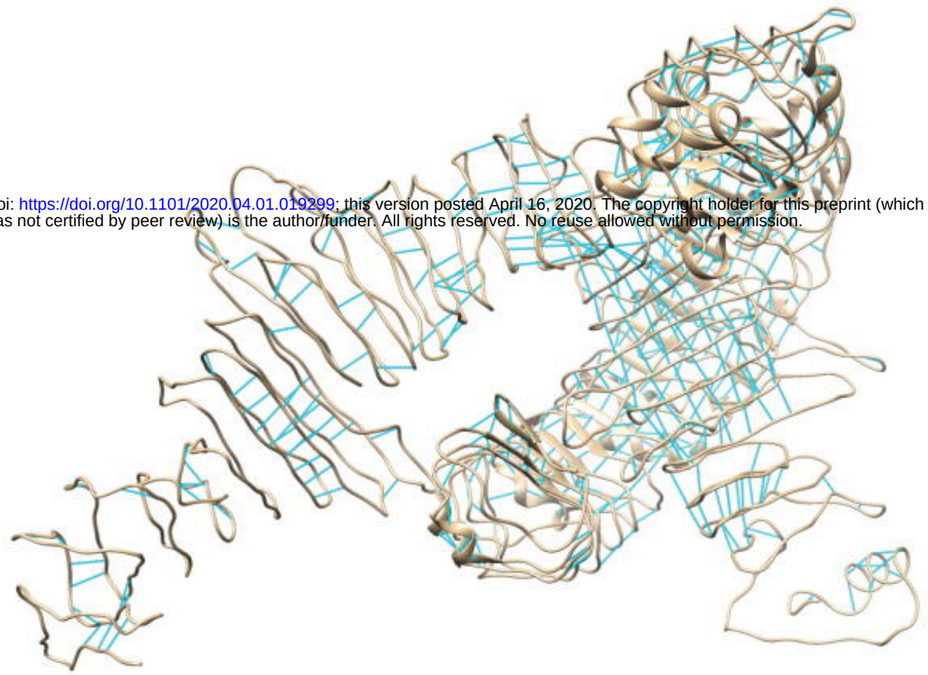

B.

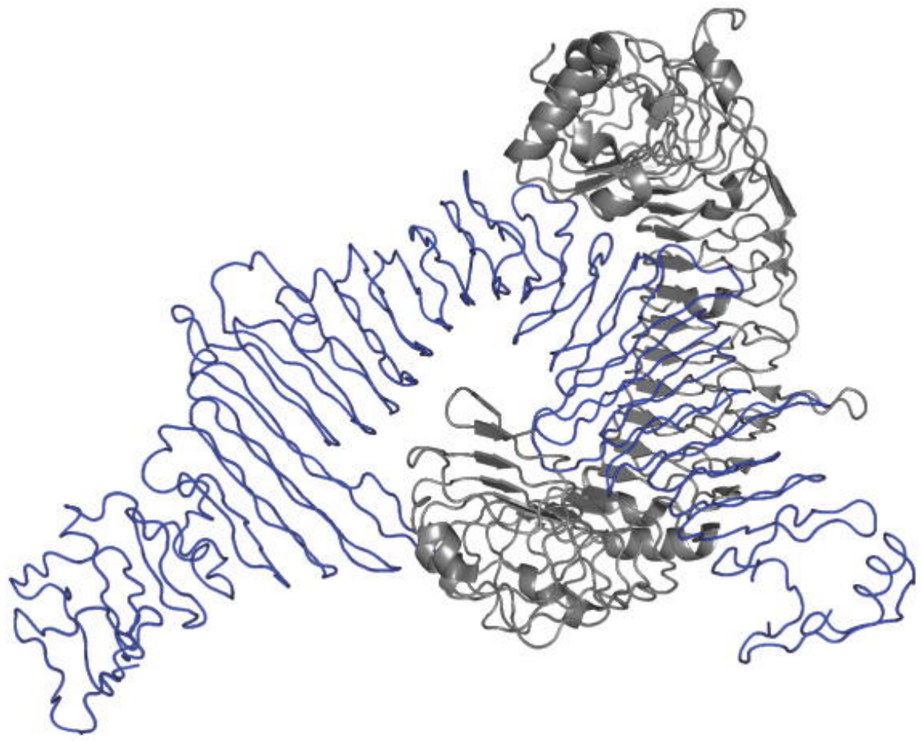

CTL Multi-epitope vaccine model in complex with TLR3

C.

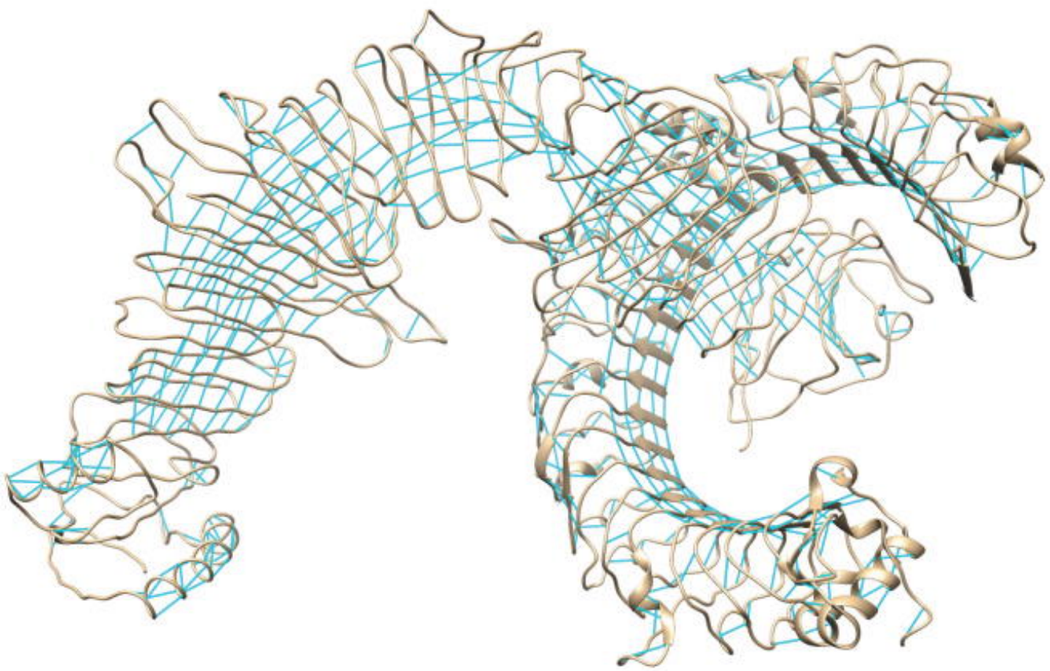

D.

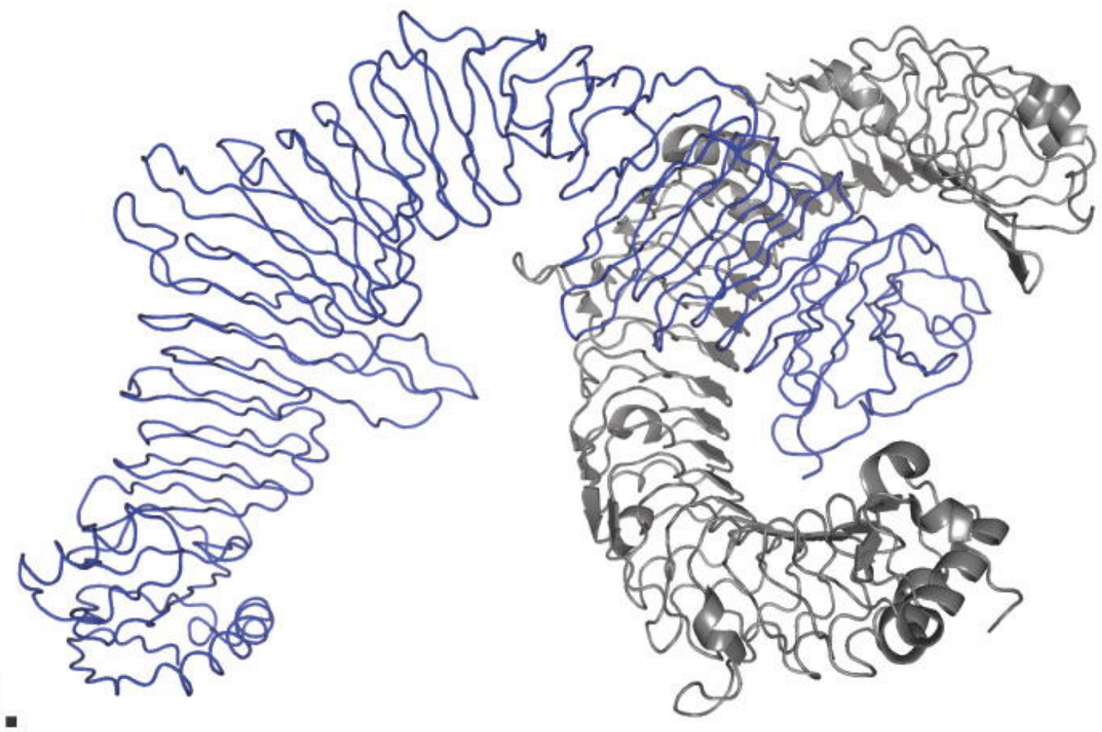

HTL Multi-epitope vaccine model in complex with TLR3

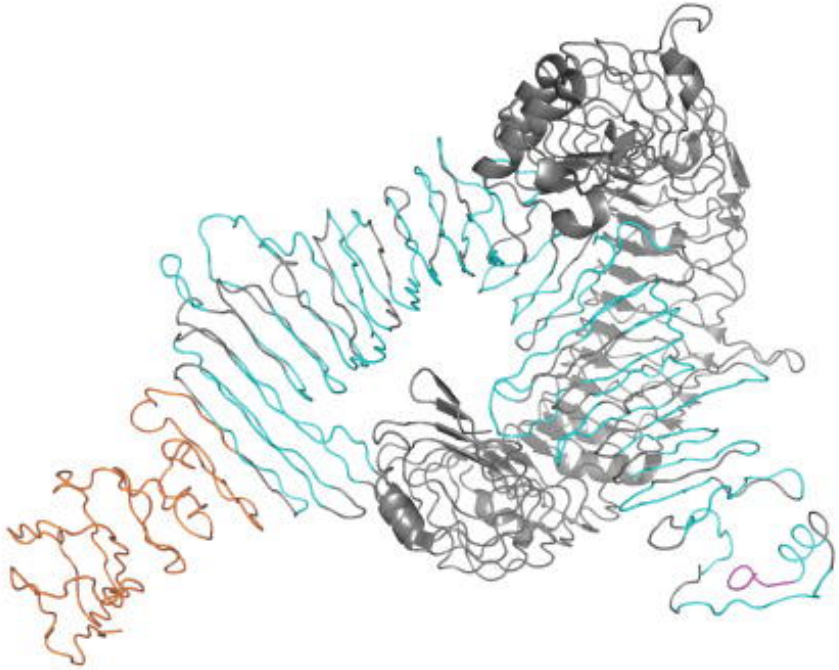

CTL Multi-epitope COVID19 vaccine
- Toll Like Receptor 3 complex

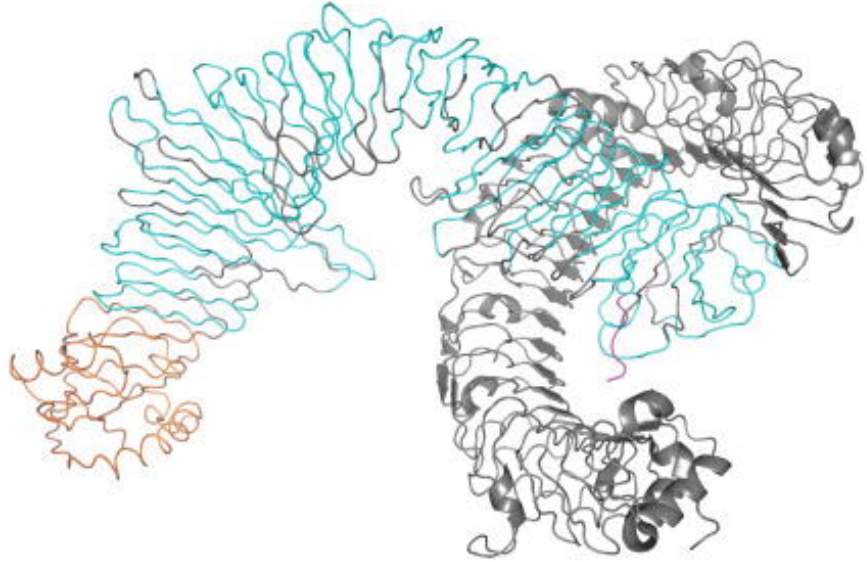

HTL Multi-epitope COVID19 vaccine
- Toll Like Receptor 3 complex

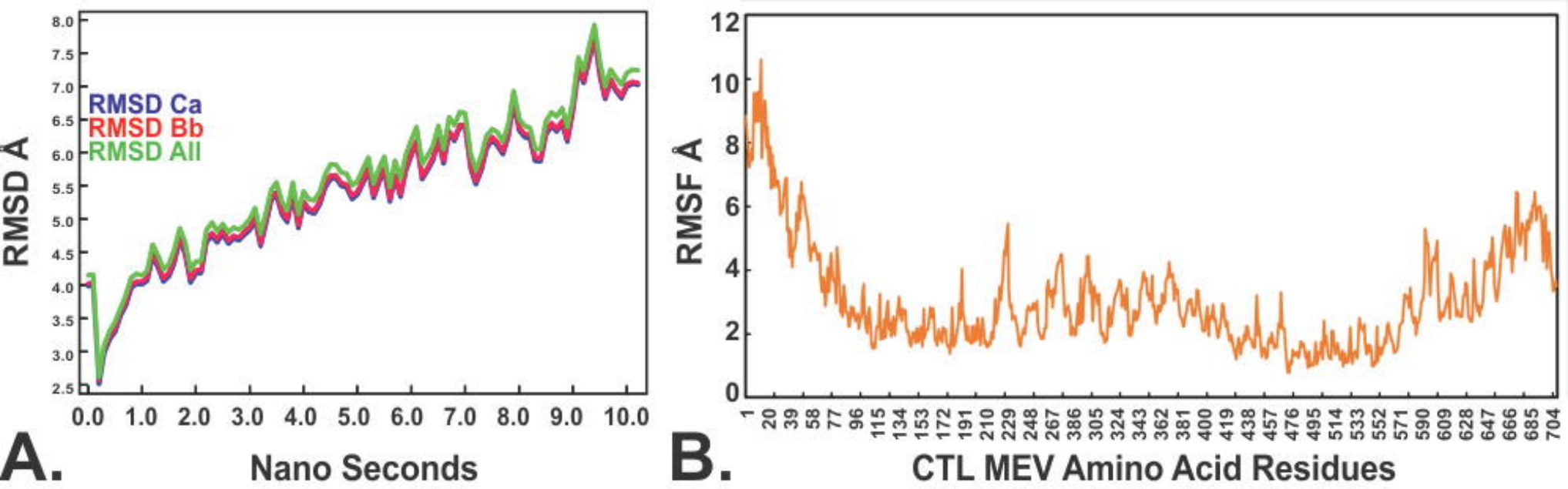

CTL Multi-epitope COVID19 vaccine - Toll Like Receptor 3 complex

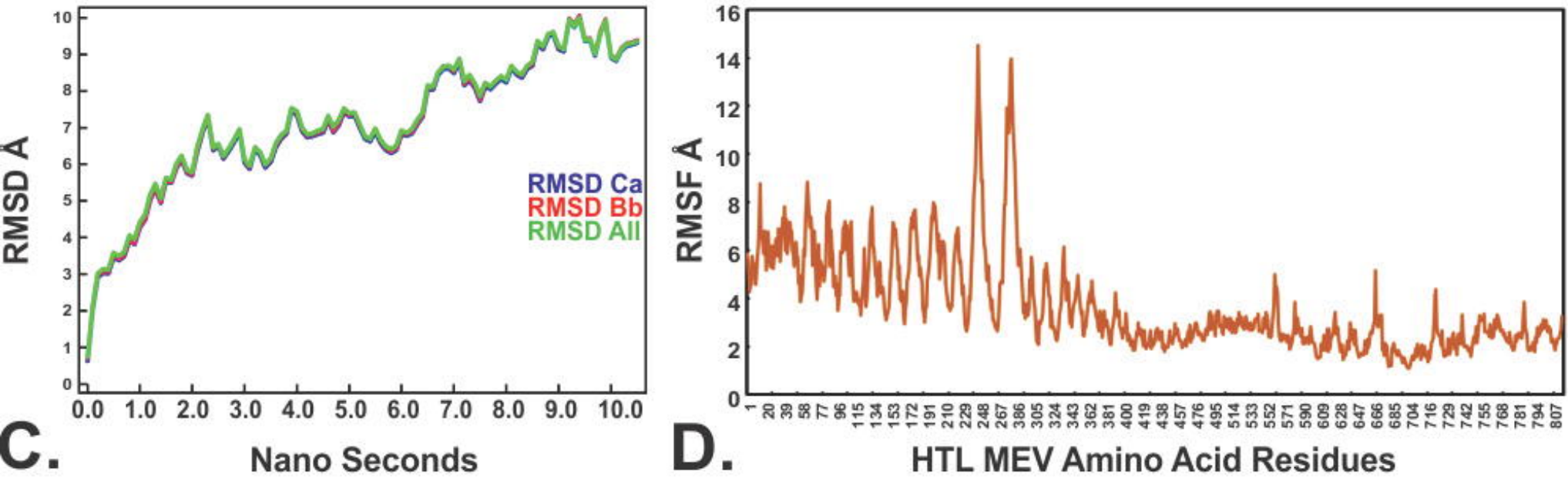

HTL Multi-epitope COVID19 vaccine - Toll Like Receptor 3 complex